A conserved lysine/arginine-rich motif in potyviral 6K1 protein is key in engaging autophagy-mediated self-degradation for completing pepper veinal mottle virus infection

Running title: Pro-viral role of cellular autophagy in viral infection

Weiyao Hu,[a] Changhui Deng,[a] Li Qin,[a] Peilan Liu,[a] Linxi Wang,[a] Xiaoqin Wang,[a] Wei Shi,[a] Asma Aziz,[a] Fangfang Li,[b] Xiaofei Cheng,[c] Aiming Wang,[d] Zhaoji Dai,[a#] Xiaohua Xiang,[e#] Hongguang Cui[a#]

[a]Key Laboratory of Green Prevention and Control of Tropical Plant Diseases and Pests (Ministry of Education) and School of Tropical Agriculture and Forestry, Hainan University, Haikou, China; [b]State Key Laboratory for Biology of Plant Diseases and Insect Pests, Institute of Plant Protection, Chinese Academy of Agricultural Sciences, Beijing, China; [c]College of Plant Protection/Key Laboratory of Germplasm Enhancement, Physiology and Ecology of Food Crops in Cold Region of Chinese Education Ministry, Northeast Agricultural University, Harbin, China; [d]London Research and Development Centre, Agriculture and Agri-Food Canada, London, Ontario, Canada; [e]Haikou Cigar Research Institute, Hainan Provincial Branch of China National Tobacco Corporation, Haikou, China.

#Correspondence: zhaoji.dai@hainanu.edu.cn; xiangxiaohuacaas@163.com; hongguang.cui@hainanu.edu.cn.

Weiyao Hu, Changhui Deng, and Li Qin contributed equally to this work. Position was determined by ascending chronological order based on the time in which these authors started with the project.

Abstract: 240 words; **Importance:** 129 words; **Article:** 5750 words; **Materials and Methods:** 1550 words.

ABSTRACT

Potyviruses possess one positive-sense single-stranded RNA genome mainly with polyprotein processing as their gene expression strategy. The resulting polyproteins are proteolytically processed by three virus-encoded proteases into 11 or 12 mature proteins. One of such, 6-kDa peptide 1 (6K1), is an understudied viral factor. Its function in viral infection remains largely mysterious. This study is to reveal part of its roles by using pepper veinal mottle virus (PVMV) as a model virus. Alanine substitution screening analysis revealed that 15 out of 17 conserved residues across potyviral 6K1 sequences are essential for PVMV infection. However, 6K1 protein is less accumulated in virus-infected cells, even though P3-6K1 junction is efficiently processed by NIa-Pro for its release, indicating that 6K1 undergoes a self-degradation event. Mutating the cleavage site to prevent NIa-Pro processing abolishes viral infection, suggesting that the generation of 6K1 along with its degradation might be important for viral multiplication. We corroborated that cellular autophagy is engaged in 6K1's degradation. Individual engineering of the 15 6K1 variants into PVMV was performed to allow for their expression along with viral infection. Five of such variants, D30A, V32A, K34A, L36A, and L39A, significantly interfere with viral infection. The five residues are enclosed in a conserved lysine/arginine-rich motif; four of them appear to be crucial in engaging autophagy-mediated self-degradation. Based on these data, we envisaged a scenario that potyviral 6K1s interact with an unknown anti-viral component to be co-degraded by autophagy to promote viral infection.

IMPORTANCE

Potyvirus is the largest genus of plant-infecting RNA viruses, which encompasses socio-economically important virus species, such as *Potato virus Y*, *Plum pox virus*, and *Soybean mosaic virus*. Like all picorna-like viruses, potyviruses express their factors mainly via polyprotein processing. Theoretically, viral factors P3 through CP, including 6K1, should share an equivalent number of molecules. The 6K1 is small in size (~6 kDa) and conserved across potyviruses, but less accumulated in virus-infected cells. This study demonstrates that cellular autophagy is engaged in the degradation of 6K1 to promote viral infection. In particular, we found a conserved lysine/arginine-rich motif in 6K1s across potyviruses that is engaged in this degradation event. This finding reveals one facet of a small protein that help understand the pro-viral role of cellular autophagy in viral infection.

KEYWORDS: *Potyvirus*, autophagy, 6K1, degradation, point mutation, pro-viral role

INTRODUCTION

Plant viruses are characterized by small genome sizes and compact structures. To overcome their limited coding capacity, viruses have evolved varied gene expression strategies to generate more functional units that are engaged in replication, encapsidation, movement, counter-defense, and transmission. *Potyvirus* is the largest genus of RNA viruses in the plant kingdom, including many well-known viral agents that adversely affect agriculturally and economically important crops, such as potato

virus Y (PVY), plum pox virus (PPV), soybean mosaic virus (SMV), and turnip mosaic virus (TuMV) (1-6). All potyviruses possess one single-stranded, positive-sense RNA genome (~9.7 kb) with a viral protein genome-linked (VPg) covalently linked to its 5′ end and a poly(A) tail at the 3′ terminus, which contains a long, full-genome open reading frame (ORF) and another relatively short ORF (PIPO) embedded in P3-coding region (7, 8). PIPO becomes translational in frame with the coding region of P1 through P3 N-terminus (P3N) from viral genomic subpopulation, which are originated from viral RNA polymerase slippage at a conserved $G_{1\text{-}2}A_6$ motif between *P3N* and PIPO during viral replication (9-11). A similar slippage event occurs in the P1-coding region for sweet potato-infecting potyviruses, giving rise to one more translational ORF (PISPO) in frame with the coding sequence of P1 N-terminus (10, 12, 13). Upon translation, the resulting polyproteins are proteolytically processed by three virus-encoded protease domains (P1, HCPro, and NIa-Pro) into 11 or 12 mature viral units, including two smallest proteins, 6-kDa peptide 1 (6K1) and 6-kDa peptide 2 (6K2) (1, 6). Intriguingly, a recent report showed that potyviral antisense genomes encode small peptides that seem to be essential for viral infectivity (14-16).

The majority of potyviral factors have been substantially studied, and the readers are referred to several recent excellent reviews that summarize their functions in viral infection (3, 4, 6, 17, 18). Potyviral 6K2 is an integral membrane protein and induces endoplasmic reticulum (ER)-derived replication vesicles that move to chloroplast for robust viral replication (19-23). In contrast, the functional roles of the other small peptide, 6K1, are less understood. The 6K1 protein was first defined over 3 decades

ago, along with *in vitro* characterization of NIa-Pro cleavage sites at P3-6K1 and 6K1-CI junctions (24, 25). The proteolytic processing at 6K1-CI junction by NIa-Pro is efficient, whereas the cleavage between P3 and 6K1 is slow, when tested in *in vitro* assays or insect cells (25-27). Thus, it was proposed that not only the mature P3 and 6K1, but also the intermediate precursor P3-6K1, are generated from corresponding genomic region (26). As anticipated, both P3 and the precursor P3-6K1 were immuno-detected in tobacco vein mottling virus-infected tobacco leaves and protoplasts by using a polyclonal antibody against P3-6K1 (24). The 6K1 as a mature protein was first detected in PPV-infected *Nicotiana benthamiana* plants via affinity-purified enrichment followed by immuno-detecting using 6K1-specific polyclonal antiserum (28). The 6K1 sequence seems pivotal for viral multiplication. Kekarainen and colleagues adopted transposition-based *in vitro* insertional mutagenesis strategy to generate a genomic 15-bp insertion mutant library based on potato virus A (PVA), and demonstrated that four insertions in the 5'-terminus of *6K1* cistron compromised viral replication (29). In addition, individual deletion of four different motifs in PPV 6K1 abolish viral replication (30). For tobacco vein banding mosaic virus, the mutations introduced into a conserved RSD motif in the middle region of 6K1 inhibited viral replication (31). Importantly, PPV 6K1 is required for viral replication and forms punctate inclusions that target 6K2-induced viral replication complex (VRC) at the early stage of infection (30). In addition, a recent report revealed a counter-defense role of PVY 6K1 via interfering with the interaction of 14-3-3h and TCTP in *N. benthamiana* (32).

Nevertheless, a comprehensive investigation on the expression of 6K1 during viral infection and its biological relevance is needed.

Autophagy is an evolutionarily conserved intracellular degradation pathway, by which the damaged or unwanted intracellular components are engulfed by *de novo*-formed double-membrane vesicles (termed autophagosomes) and subsequently delivered to vacuoles for breakdown and turnover in plants (33-35). Numerous recent studies demonstrate that autophagy is engaged in plant defense responses against viruses (including potyviruses), and in turn, viruses evolve strategies to counteract, manipulate or hijack autophagy pathway to promote viral infection (36-38). Potyviral HCPro functions as viral suppressor of RNA silencing (VSR), mainly via directly interacting with, and kidnapping, virus-derived small interfering RNAs (vsiRNAs) (39). Tobacco calmodulin-like protein (rgs-CaM) targets dsRNA-binding domain in HCPro and cooperates with autophagy pathway to degrade HCPro (40). NBR1, a canonical cargo receptor in selective autophagy, targets TuMV HCPro-induced RNA granules for autophagic degradation to suppress viral accumulation (41). Beclin1/ATG6, a core component of phosphoinositide-3-kinase (PI3K) complex, interacts with TuMV NIb and mediates its autophagic degradation likely through an adaptor ATG8a (42).

However, several studies revealed the pro-viral roles of autophagy in potyviral infection. VPg is another potyvirus-encoded VSR, which functions through interacting with suppressor of gene silencing 3 (SGS3, a core component in dsRNA synthesis) to mediate the degradation of SGS3 and RNA-dependent RNA polymerase 6 (RDR6) via both the ubiquitin-proteasome and autophagy pathways (43). Group 1 Remorins (REMs)

negatively regulate the cell-to-cell movement of TuMV. To survive, virus-encoded VPg interacts with REM1.2 to degrade it via both 26S ubiquitin–proteasome and autophagy pathways (44). TuMV activates and manipulates NBR1-ATG8f autophagy in an UPR-dependent manner to anchor VRC to the tonoplast to promote viral replication and virion accumulation (45). Interestingly, TuMV P1 protein interacts with a chloroplast protein cpSRP54 to mediate its degradation via the ubiquitin-proteasome and autophagy pathways to suppress jasmonic acid (JA) biosynthesis and enhance viral infection (46). Therefore, the complicated interactions between potyvirus and autophagy pathway deserve further investigations.

As summarized, potyviral 6K1 is an understudied viral unit, in particular that its expression profile and biological relevance await further investigations. We performed a comprehensive alanine substitution screening, and identified 15 conserved residues in 6K1 sequence that are essential for the infection of pepper veinal mottle virus (PVMV, *Potyvirus* genus). However, 6K1 protein undergoes a degradation event and is less accumulated in virus-infected cells. We demonstrated that cellular autophagy is engaged in 6K1's degradation. Moreover, we identified four residues enclosed in a conserved lysine/arginine-rich motif in potyviral 6K1s, which are engaged in the autophagy-mediated degradation for the promotion of viral infection.

RESULTS

Construction of a GFP-tagged PVMV clone

For potyviruses, both P1/HC-Pro and NIb/CP intercistronic sites are widely engineered to express heterologous proteins (4, 47). To visually monitor PVMV infection, we employed the infectious cDNA clone of the isolate PVMV-HNu (termed pHNu) (48) as the backbone to integrate a complete *GFP* sequence into NIb/CP junction. The resulting clone was designated as pHNu-GFP (Fig. 1A). The original cleavage site 'DFVLHQ/AG' at NIb/CP junction (recognized by NIa-Pro) was introduced into both NIb/GFP and GFP/CP junctions for the release of free GFP along with viral genome expression. To examine the infectivity of pHNu-GFP, *N. benthamiana* and *Capsicum chinense* seedlings (n = 8 per plant species) were inoculated with pHNu-GFP via agro-infiltration. At 5 days post-inoculation (dpi), *N. benthamiana* plants started to show green fluorescence signals along veins in top non-inoculated leaves under UV lamp (Fig. 1B). The strong fluorescence signals were observed in top leaves for all inoculated plants at 10 dpi and 30 dpi (Fig. 1B). For all *C. chinense* plants inoculated with pHNu-GFP, obvious fluorescence signals were shown at 10 dpi and 15 dpi (Fig. 1C). Similar with pHNu (48), pHNu-GFP induces severe symptoms (such as foliar chlorosis and rugosity, and dwarfism in size) in both *N. benthamiana* and *C. chinense*. Furthermore, the upper non-inoculated leaves of diseased *N. benthamiana* and *C. chinense* plants were harvested for immunodetection of GFP. As anticipated, a major band corresponding to the putative size of free GFP (~27.7 kDa) was detected in infected leaves (Fig. 1D), indicating that free GFP is efficiently processed and released from viral genome-encoded polyprotein by NIa-Pro.

Fifteen out of 17 conserved residues across potyviral 6K1s are essential for PVMV infection in *N. benthamiana* or *C. chinense*

To investigate the biological significance of 6K1 sequence during viral infection, a total of 115 sequences of 6K1 from different potyviruses were retrieved from NCBI GenBank database, and subjected to multiple alignment analysis. The results showed that potyviral 6K1 sequences are rather conserved. A total of 17 highly-conserved residues, excluding the conserved Gln at the position P1 of NIa-Pro cleavage site at 6K1-CI junction, were characterized: Lys / Arg (K3, 38; K/R28, 34, 40), Asp / Glu (E11; D25, 30; D/E27), Ala (A15), Leu (L19, 36, 39), Met (M22), Ser (S29), and Val (V32, 51) (Fig. 2A). We performed alanine substitution screening to evaluate the effects of these conserved residues on viral infectivity. For A15, it was substituted with Arg. Using pHNu-GFP as the backbone, we produced a total of 17 mutated clones, by which the resulting virus mutants are expected to harbor single substitution of conserved residues in 6K1 with Ala, or A15 with Arg. For the convenience of description, pHNu-GFP is designated as WT in this section. These mutated clones, together with WT, were individually inoculated into both *N. benthamiana* (n = 8 per clone) and *C. chinense* seedlings (n = 5 per clone) by agro-infiltration.

In *N. benthamiana*, all plants inoculated with WT(S29A) or WT(V51A) exhibited severe distortion symptoms and strong GFP signals in top leaves at 10 dpi, resembling those inoculated with WT. Two of five plants inoculated with WT(V32A) showed mild symptoms and weak GFP signals (Fig. 2B). Neither virus-infected symptoms nor GFP signals were observed on plants inoculated with the other mutated clones at this time

point (Fig. 2B, 2F, and Fig. S1). Intriguingly, clear GFP signals started to show in top leaves of three out of five plants inoculated with WT(K40A) at 19 dpi (Fig. 2B). Except the plants mentioned above, the remaining ones did not show any discernible symptom or GFP signals, even until 30 dpi. For virus progeny derived from WT(S29A), WT(V32A), WT(K40A), and WT(V51A), the genomic sequence, covering P3 C-terminus, 6K1, and CI N-terminus, was determined. Spontaneous mutations were not found for both WT(S29A) and WT(V51A). However, one reversion mutation 'C to T', leading to 'A to V' at position 32 was identified for the progeny of WT(V32A) (Fig. 2C). For the progeny of WT(K40A), a compensatory mutation 'G to A', resulting in 'G to R' at position 44, took place (Fig. 2C). Taken together, the above results confirm that all conserved residues across potyviral 6K1s, excluding S29 and V51, are key for a successful infection of PVMV in *N. benthamiana*.

In *C. chinense*, all plants inoculated with WT(S29A) or WT(K40A) displayed strong GFP signals in top leaves at 15 dpi, resembling WT-inoculated plants (Fig. 2D). Intriguingly, strong GFP signals appeared in top leaves of two WT(V32A)-inoculated and one WT(A15R)-inoculated plants at 25 dpi (Fig. 2D). Except the plants mentioned above, the remaining plants did not show GFP signals (Fig. 2D, 2F, and Fig. S2), even until 45 dpi. Similarly, the genomic sequences surrounding 6K1 for viral progeny were determined. No spontaneous mutations were found for the progeny of WT(S29A) and WT(K40A). In line with the observation in *N. benthamiana*, the reversion mutation 'A to V' at position 32 was found for the progeny of WT(V32A) (Fig. 2E). For the progeny of WT(A15R), one mutation 'C to G', resulting in 'R to G' at position 15, was observed

(Fig. 2E). Collectively, all conserved residues in 6K1s, with the exception of S29 and K40, are essential for PVMV infection in its natural host, *C. chinense*.

6K1 protein is less accumulated during PVMV infection

To examine the expression dynamics of mature 6K1 in viral infection, we created a modified virus clone, pHNu-GFP-6K1^{Myc}, to express a C-terminal Myc-fused 6K1 (Fig. 3A). Infectivity test showed that the plants inoculated with pHNu-GFP-6K1^{Myc} exhibited similar symptoms and distribution pattern of GFP signals with those treated with pHNu-GFP in *N. benthamiana* (Fig. 3B). The presence of virus in upper non-inoculated leaves was confirmed by RT-PCR (Fig. 3C). For the virus progeny, the sequence spanning the Myc tag was determined, and spontaneous mutations / deletions were not observed (Fig. 3D), indicating that the attachment of Myc epitope at the C-terminus of 6K1 has no obvious effect on viral infectivity. Both inoculated (IL) and upper non-inoculated leaf (TL) samples were harvested at different time points, and subjected to immunodetection of 6K1^{Myc}. The results showed that a specific band corresponding to the putative size of the precursor P3-6K1^{Myc} (~47.0 kDa) was detected not only from IL samples at 5 dpi and 6 dpi, but also from TL samples at 5 dpi, 6 dpi, and 7 dpi (Fig. 3E). However, the mature 6K1^{Myc} (~7.6 kDa) was not immuno-detected at all these time points (Fig. 3E), implying that a low abundance of 6K1 protein, at an undetectable level by immunoblotting, is along with viral infection.

P3-6K1 junction is efficiently processed by NIa-Pro in viral infection

Previously studies based on *in vitro* assays or in insect cells showed that 6K1-CI junction in potyviral polyprotein was efficiently processed by NIa-Pro but the

processing at P3-6K1 junction at a low rate (25-27). These observations compeled us to speculate that a low abundance of 6K1 during PVMV infection might be the consequence of low-efficient cleavage by NIa-Pro at P3-6K1 junction. To test this idea, we examined the processing efficiency of P3-6K1 junction in viral infection. We created a modified virus clone, pHNu-GFP-^{Myc}P3, to express N-terminal Myc-fused P3 or P3-6K1 (if have) (Fig. 3A). The clone was inoculated into *N. benthamiana* seedlings (n = 10). The results showed that pHNu-GFP-^{Myc}P3 behaved like pHNu-GFP, in terms of symptom phenotype and GFP distribution pattern in upper non-inoculated leaves (Fig. 3B). Viral infection in upper non-inoculated leaves were confirmed by RT-PCR (Fig. 3C). The sequence spanning the Myc tag for virus progeny was determined, and spontaneous mutations / deletions were not found (Fig. 3D), indicating that the fusion of Myc epitope with the N-terminus of P3 has no discernible effect on viral infectivity. Leaf samples were harvested from upper non-inoculated leaves at 5 and 6 dpi, and used for immunodetection with anti-Myc polyclonal antibody. Two specific protein bands with the putative size for ^{Myc}P3-6K1 (~46.8 kDa) and ^{Myc}P3 (~40.7 kDa) were detected (Fig. 3F). However, the signal intensity of the band representing ^{Myc}P3 was markedly higher than that of ^{Myc}P3-6K1 (Fig. 3F), indicating that P3-6K1 junction is efficiently processed by NIa-Pro during PVMV infection. In combination of the data in previous section, it is suggesting that PVMV 6K1 is efficiently released from viral polyprotein, but undergoes an intracellular self-degradation event.

Proteolytic processing at P3-6K1 junction is indispensable for the successful infection of PVMV

Next, we tested whether the processing of viral polyprotein at P3-6K1 junction is required for viral infection. Previous studies based on *in vitro* assays showed that amino acid substitution in conserved heptapeptide recognized by NIa-Pro alters or disables the efficiency of proteolytic processing (26, 49). Substitution of Gln with His at P1 position blocks the processing by NIa-Pro (26, 50). Replacement with Lys at P1′ position disturbs NIa-Pro processing (51). Statistically, Gln is the most frequent residue at P1 position, whereas Ala is absent at this position. At P1′ position, Ala, Ser and Gly are the most frequent residues, but Gln is absent (49).

Based on the above observations, five substitutions, Q-H, A-K, QA-AQ, Q-A, and A-Q, were individually introduced into the heptapeptide at P3-6K1 junction by using pHNu-GFP-^{Myc}P3 as the backbone, to destroy the cleavage of NIa-Pro at P3-6K1 junction (Fig. 4A). All mutated clones were inoculated into *N. benthamiana* seedlings (n = 8 per clone). As shown in Fig. 4B, sorely pHNu-GFP-^{Myc}P3(A-Q), behaving like PVMV-GFP-^{Myc}P3, was aggressive in *N. benthamiana*. Further, we examined the cleavage of NIa-Pro at P3-6K1 junction for these mutants *in planta*. The inoculated leaves were harvested at 5 dpi for immunoblotting detection with anti-Myc polyclonal antibody. The results showed that both ^{Myc}P3 and ^{Myc}P3-6K1 were detected for pHNu-GFP-^{Myc}P3(A-Q) and pHNu-GFP-^{Myc}P3 (Fig. 4D), indicating that the P3-6K1 junction for them is processed by NIa-Pro in viral infection. Noticeably, the signal intensity of the band corresponding to ^{Myc}P3 is much weaker than that of P3-6K1 for PVMV-GFP-^{Myc}P3(A-Q), suggesting a relatively low processing efficiency at the mutated cleavage site. Unfortunately, either P3-6K1 or P3 was not detected for the other four mutants

(Fig. 4D). A most likely explanation is that these introduced mutations prevent NIa-Pro's cleavage at P3-6K1 junction, compromise viral multiplication, and contribute to the accumulation of P3-6K1 at an undetectable level.

Intriguingly, GFP signals started to emerge in top leaves of one plant inoculated with pHNu-GFP-^{Myc}P3(A-K) at 21 dpi, and became strong at 30 dpi (Fig. 4C), indicating that virus progeny derived from this clone are infectious in *N. benthamiana*. For the virus progeny, the sequence surrounding P3-6K1 junction was determined. A spontaneous nucleotide mutation, leading to the reversion from Lys to Asn at P1′ position, was detected. We proposed that the spontaneous mutation might recover the cleavage of NIa-Pro at P3-6K1 junction, leading to viral successful infection. To test this idea, the substitution with Asn at P1′ position was introduced (Fig. 4A) to generate the clone pHNu-GFP-^{Myc}P3(A-N). The infectivity of the clone was greatly recovered, evidenced by that all eight inoculated plants exhibited severe leaf rugosity symptoms and strong GFP signals in top leaves, resembling the plants inoculated with pHNu-GFP-^{Myc}P3 (Fig. 4B). The expression of both P3 and P3-6K1 was examined. The result showed that both proteins were immuno-detected, indicating the reversion mutation 'K to N' at P1′ position recover, albeit partially, the cleavage at P3-6K1 junction, and, thus, rescue viral infectivity.

Collectively, the above results support the notion that proteolytic processing at P3-6K1 junction is indispensable for viral successful infection. In combination with the observation that 6K1 is less accumulated in viral infection (Fig. 3), it is speculated that

312 the generation of mature 6K1 along with its intracellular degradation might be
313 important for viral infection.

314 **PVMV 6K1 undergoes autophagic degradation**

315 Potyviral 6K1s, when ectopically expressed *in planta*, diffuse into cytoplasm and
316 nucleus (30, 31, 52, 53). Once expressed in the context of viral infection, they would
317 form functional punctate structures targeting 6K2-induced replication vesicles (30, 31).
318 This prompted us to investigate, in the context of viral infection, the mechanism by
319 which PVMV 6K1 is degraded. For the convenience of the detection of 6K1, we
320 engineered a second copy of 6K1 with its C-end fused with GFP into NIb-CP junction
321 of pHNu to generate a recombinant clone, pHNu//6K1-GFP) (Fig. 5A). The attachment
322 of a GFP-tag to the C-terminus of 6K1 seems not affect its colocalization with 6K2-
323 induced replication vesicles (30). The recombinant clone enables our detection of 6K1
324 in the context of viral infection. Autophagy and ubiquitin-proteasome machineries are
325 two main intracellular degradation pathways (54, 55). We selected two autophagy
326 inhibitors, 3-methyladenine (3-MA) and E-64d, and a 26S proteasome inhibitor MG132
327 to determine the effects of autophagy and ubiquitin-proteasome pathways on the
328 degradation of 6K1. Agrobacterial cultures harboring pHNu-GFP (as the parallel
329 control) or pHNu//6K1-GFP (OD_{600} = 1.0 per culture) were primarily inoculated into
330 fully-expanded leaves of *N. benthamiana* seedlings at 6- to 8-leaf stage. At 80 hours
331 post-inoculation (hpi), the inoculated leaves were treated with different chemical
332 inhibitors (Fig. 5B). Sixteen hours later, the treated leaves were sampled for
333 immunoblotting analysis. E-64d treatment significantly increased the accumulation of

6K1-GFP, whereas the treatment did not obviously alter the accumulation of free GFP in the parallel control (Fig. 5C). The results suggest that cellular autophagy is engaged in the degradation of 6K1 in viral infection. Even though MG132 treatment enhanced the abundance of 6K1-GFP, the enhancing effect was also observed for free GFP in the parallel control (Fig. 5C). Herein, it could not be concluded whether the ubiquitin-proteasome pathway is engaged in 6K1's degradation. In contrast with E-64d, the treatment with 3-MA had no increasement effect on the accumulation of 6K1-GFP (Fig. 5C).

Previous studies reported that potyviral 6K1s form punctate structures that target 6K2-induced VRC in virus-infected cells (30, 31). The colocalization of PVMV 6K1 with 6K2-induced VRC was tested. Agrobacterial culture harboring pHNu//6K1-GFP (0.5 of OD_{600}) was infiltrated into *N. benthamiana* leaves, which, at 24 hpi, were re-inoculated with an agrobacterial culture harboring pCaM-6K2-mCherry (0.3 of OD_{600}). Thirty-six hours later, 6K1-GFP forms punctate structures, which largely co-localize with 6K2-mCherry vesicles (Fig. 5D). When autophagy pathway is activated, ATG8 proteins ectopically expressed *in planta* would form punctate structures representing autophagosomes (42, 56, 57). Both ATG8a and ATG8f from *N. benthamiana* with their N-ends fused with mCherry (mCherry-NbATG8a and mCherry-NbATG8f) were used as autophagosome markers to further dissect the association of 6K1 with autophagic event. The agrobacterial culture harboring pHNu//6K1-GFP, together with the culture containing pCaM-mCherry-NbATG8a or pCaM-mCherry-NbATG8f (final OD_{600} = 0.25 per culture), were co-inoculated into fully-expanded leaves of *N. benthamiana*

356 seedlings at 6- to 8-leaf stage. Indeed, a portion of punctate structures formed by 6K1-
357 GFP co-localized with mCherry-NbATG8a or mCherry-NbATG8f structures in
358 cytoplasm (Fig. 5E). These data indicate that 6K1 is physically associated with ATG8s-
359 labled autophagosomes during viral infection.

360 To further determine the degradation of 6K1 by cellular autophagy, we constructed
361 one hairpin RNAi construct (p2300s-intron-dsATG7) for the transient silencing of
362 *NbATG7* to block cellular autophagy pathway, and another one p2300s-intron-dsGUS
363 as the parallel control. Meanwhile, a T-DNA construct (pCaM-6K1-GFP) for transient
364 expression of 6K1-GFP was developed. Agrobacterial cultures, harboring
365 corresponding pCaM-6K1-GFP and p2300s-intron-dsATG7 or p2300s-intron-dsGUS
366 (final OD_{600} = 0.3 per culture) were co-infiltrated into fully-expanded leaves of *N.*
367 *benthamiana* seedlings at 6- to 8-leaf stage (Fig. 5F). Seventy-two hours later, the
368 mRNA transcripts of *NbATG7* in inoculated leaves with the combination of p2300s-
369 intron-dsATG7 and pCaM-6K1-GFP was reduced by 76%, compared with the parallel
370 control (Fig. 5G). In turn, an increasing amount of 6K1-GFP by 73%, in comparison
371 with that from the parallel control, was detected (Fig. 5H).

372 **Individual expression of five 6K1 variants (D30A, V32A, K34A, L36A, and L39A)**
373 **along with viral infection significantly interfere with viral infection progression;**
374 **the five residues are encompassed in a Lys/Arg-rich motif across potyviral 6K1s**

375 Herein, we hypothesized that: i) the degradation of 6K1 by cellular autophagy might
376 be important for viral infection; ii) there might be the existence of potential amino acid(s)
377 or motif(s) in 6K1 that determine its autophagic degradation, and mutating these

residues would interfere with viral infectivity. To test the ideas, the fifteen *6K1* variants (Fig. 2) were individually engineered into pHNu at the intercistronic junction of *NIb* and *CP* (Fig. 6A). Each of the resulting recombinant clones were inoculated into three *N. benthamiana* seedlings at 9- to 10-leaf stage (OD_{600} = 0.1 per clone). At 5 dpi, all plants inoculated with pHNu//6K1 exhibited obvious vein-clearing and distortion symptoms in top leaves (Fig. 6B). Similar symptoms were also observed in plants inoculated with pHNu//6K1 variants (K3A, E11A, A15R, M22A, D25A, D27A, and K38A) (Fig. S3A). However, virus-induced symptoms were not discernible in plants inoculated with pHNu//6K1 variants (L19A, R28A, D30A, V32A, K34A, L36A, L39A, and K40A) at this time point (Fig. 6B). In line with above observations, a significantly lower abundance of viral genomic RNAs was detected from plants inoculated with these clones, with the exception of pHNu//6K1(L19A) (Fig. 6C). It was noticed that all pHNu//6K1 variants, behaving like pHNu//6K1, induced nearly-consistent severe symptoms at 7 dpi (Fig. S3B). Consistently, a comparable level of viral RNA accumulation was shared by all pHNu//6K1 variants and pHNu//6K1 at this time point (Fig. S3C). Conclusively, individual expression of seven 6K1 variants (R28A, D30A, V32A, K34A, L36A, L39A, and K40A) significantly delays viral infection progression in *N. benthamiana*, likely via interfering with the function of the cognate 6K1 in PVMV.

Further, the performance of the seven recombinant clones in *C. chinense* was investigated. These pHNu//6K1 variants, together with pHNu//6K1, were each inoculated into six *C. chinense* plants at 5- to 6-leaf stage (OD_{600} = 0.1 per clone). All plants inoculated with pHNu//6K1(R28A), or pHNu//6K1(K40A), similar with the

plants inoculated with pHNu//6K1, exhibited obvious virus-induced symptoms at 10 dpi, such as chlorosis along veins in upper non-inoculated leaves (Fig. 6D). In contrast, no or mild symptoms were observed in plants inoculated with pHNu//6K1 variants (D30A, V32A, K34A, L36A, and L39A) (Fig. 6D). In accordance, a significantly lower viral RNA accumulation level was detected for the groups of plants showing no or mild symptom (Fig. 6E). Similar with what was observed in *N. benthamiana*, all *C. chinense* plants inoculated with each of pHNu//6K1variants or pHNu//6K1 exhibited indistinguishable severe symptoms at 15 dpi (Fig. S3D). A comparable level of viral RNA accumulation was shared by these pHNu//6K1 variants and pHNu//6K1 at this time point (Fig. S3E).

Taken together, individual expression of five 6K1 variants (D30A, V32A, K34A, L36A, and L39A) along with viral infection greatly hinders viral infection progression in both *N. benthamiana* and *C. chinense*. Further analysis revealed that the five conserved residues are encompassed in a Lys/Arg-rich motif across potyviral 6K1s (Fig. 2A).

The four conserved residues (V32, K34, L36, L39) across potyviral 6K1s are related with the autophagic degradation of PVMV 6K1

Next, we investigated whether the five conserved residues (D30, V32, K34, L36, and L39) are engaged in the autophagic degradation of PVMV 6K1. To test this hypothesis in the context of viral infection, individual substitution of them with alanine was introduced into 6K1-GFP in pHNu//6K1-GFP (Fig. 7A). The obtained clones pHNu//6K1 variants-GFP together with pHNu//6K1-GFP were each inoculated into

422 fully-expanded leaves of *N. benthamiana* leaves at 6- to 8-leaf stage (OD_{600} = 1.0 per
423 culture). At 80 hpi, the inoculated leaves were treated with E-64d or DMSO (Fig. 7B).
424 Sixteen hours later, the treated leaves were sampled for immunoblotting analysis. The
425 results showed that E-64d treatment failed to enhance the accumulation of 6K1(D30A)-
426 GFP, 6K1(V32A)-GFP, 6K1(K34A)-GFP, 6K1(L36A)-GFP, or 6K1(L39A)-GFP,
427 which was in contrast with 6K1-GFP in pHNu//6K1-GFP (Fig. 7C).

428 To further evaluate the association of the five residues with autophagic degradation
429 of 6K1, individual substitution of them with alanine was introduced into 6K1-GFP in
430 pCaM-6K1-GFP. Each agrobacterial culture harboring relevant plasmids was co-
431 infiltrated with p2300s-intron-dsATG7 or p2300s-intron-dsGUS into fully-expanded
432 leaves of *N. benthamiana* seedlings at 6- to 8-leaf stage (Fig. 7D). Seventy-two hours
433 later, the co-inoculated leaves were sampled for immunoblotting analysis. The results
434 showed that the treatment with dsATG7 construct failed to enhance the accumulation
435 of 6K1(V32A)-GFP, 6K1(L36A)-GFP, and 6K1(L39A)-GFP, when compared with the
436 treatment by dsGUS. The dsATG7 treatment increased the amount of 6K1(K34A)-GFP
437 by 50% (Fig. 7E). However, the treatment by dsATG7 construct yielded approximately
438 two-fold amount of 6K1(D30A)-GFP, similar with the case of 6K1-GFP (Fig. 7E). The
439 molecular mechanism underpinning the contrasting effects of D30 on 6K1's autophagic
440 degradation (transient expression versus the expression in viral infection) (Fig. 7C, 7E),
441 awaits to be further investigated. Collectively, four 6K1 variants (V32A, K34A, L36A,
442 and L39A) inhibited the autophagic degradation of 6K1.
443

DISCUSSION

During co-evolution between viruses and plant hosts, the end-less arm races are launched. To survive, viruses continuously forge a limited number of self-encoded proteins via genetic variation / evolution to counteract host multi-layered defensive responses, including but not limited to RNA silencing and cellular autophagy. The 6K1 is one of the most evolutionarily-conserved proteins among potyviruses, but its biological relevance is less annotated. This study demonstrates that most of conserved residues in potyviral 6K1s are essential for a successful infection of PVMV. We provide multi-disciplinary evidence supporting that cellular autophagy is engaged in the degradation of 6K1. We defined a conserved lysine/arginine-rich motif in 6K1s across potyviruses that is responsible for the autophagy-mediated self-degradation to promote viral infection. This finding provides a new insight in our understanding of a conserved but understudied potyviral protein.

Numerous studies demonstrate that autophagy plays dual roles during virus-plant interactions (36-38). Regarding potyviruses, autophagy-mediated degradation of key viral proteins such as HCPro and NIb fight against viral infection (40-42). This study proves that autophagy-mediated degradation of 6K1 facilitates viral infection, indicating a pro-viral role of autophagy in potyviral infection. Previously, there were two reports showing the facilitative effect on potyviral infectivity: i) TuMV VPg interacts with SGS3 to mediate the autophagic degradation of both SGS3 and RDR6 to promote viral infection (43); ii) TuMV P1 protein interacts with cpSRP54 to mediate its autophagic degradation to suppress JA biosynthesis (46). The two cases reveal that

potyviral proteins cooperate or co-opt cellular autophagy machinery to eliminate core proteins in antiviral pathways. Based on these observations, we envisage a scenario that 6K1 cooperate with autophagy machinery to degrade certain cellular antiviral component. To verify this hypothesis, two following questions need to be answered.

First, what is the molecular mechanism underpinning the autophagic degradation of 6K1? To address this question, it is necessary to perform a comprehensive screening of potential interactors of 6K1 to identify autophagic receptor and adaptor proteins, which will be a promising research direction. Recently, a milestone discovery for potyvirid 6K1 is that it is also an endoplasmic reticulum (ER)-localized integral membrane protein, forms pentamers with a central hydrophobic tunnel, and increases the cell membrane permeability to facilitate viral infection (58). Intriguingly, artificial intelligence-assisted structure modeling and biochemical assays demonstrated that three arginine residues, i.e., K/R34, K38, and K40 in the conserved Lys/Arg-rich motif defined in this study (Fig. 2), are responsible for its oligomerization (58). This prompted us to speculate that the four residues (V32, K34, L36, and L39) in Lys/Arg-rich motif that determine 6K1's autophagic degradation, might depend on its oligomerization. Our study emphasizes the importance of the conserved Lys/Arg-rich motif in 6K1's self-interaction for implementing critical biological functions.

Second, which components are co-degraded with 6K1 by autophagy. Interestingly, a recent study showed that transient expression of TuMV 6K1 decreases the activity of cellular cysteine proteases (59), which were demonstrated as the central hubs of plant immunity against many pathogens including viruses (60-63). SMV 6K1 interacts with

a large number of defense-related proteins from soybean, such as pathogenesis-related protein 4, Bax inhibitor 1, papain family cysteine protease, and cysteine protease inhibitors (53). PVY 6K1 interacts with 14-3-3 protein, playing a vital role in plant defense against various pathogens, including PVY (32). It seems that the known interactors of 6K1 are all categorized as defense-related proteins. Consequently, the clarification of host components co-degraded with 6K1 would unveil a novel counter-defense strategy expressed by potyviruses.

In the case of PPV, artificial inactivation of proteolytic processing at P3-6K1 junction via mutating either 'Gln to His' at P1 position or 'Ala to Lys' at P1′ position, markedly weakened viral systemic infection in *N. benthamiana*, suggesting an accessory role of 6K1 in viral multiplication (25, 26, 30). However, the effects of introduced mutations on NIa-Pro processing of P3-6K1 junction were detected in *in vitro* assays. The influences of these mutations on the processing *in planta* await to be proved. For PVMV, these mutations, when introduced into viral clones, abolished the P3-6K1 processing *in planta*, leading to a failure of viral infection. Spontaneous reversion mutation from Lys to Asn at P1′ position restored the proteolytic processing, and thus rescued viral systemic infection. These results strongly suggest that proteolytic processing at P3-6K1 junction to release mature 6K1 is required for viral successful infection. In addition, we observed that a slow processing at P3-6K1 junction had no obvious effect on viral systemic infection and symptom development (Fig. 4). Nevertheless, the correlation between the processing of P3-6K1 junction *in planta* and viral infectivity needs to be carefully examined in different potyvirus-host pathosystems.

Plant viruses characteristically have small sizes and compact genomes. To overcome the limited coding capacity, viruses evolved a variety of strategies to express more viral proteins, such as stop codon readthrough, leaky scanning, and frameshifting. In *in vitro* assays, both the cleavages at HCPro-P3 junction by HC-Pro and at 6K1-CI junction by NIa-Pro is efficient (27, 28, 64, 65), whereas the cleavage at P3-6K1 junction is slow (25, 27), suggesting the generation of three viral proteins (i.e., P3, 6K1, and P3-6K1) from corresponding genomic region (26). Consistently, all PVMV-derived clones tested in this study, if variable, expressed the precursor P3-6K1 to a varied degree (Figs. 3E, 3F, 4D, 4E). Based on these observations, we assume that: i) P3-6K1 might be also functional, which deserves further investigation. In the case of TuMV, the precursor P3-6K1 is an integral membrane protein, whereas P3 is a peripheral membrane protein; P3-6K1 forms small granules on the ER network, and might have distinct biological function(s) (58). ii) besides polyprotein processing and RNA polymerase slippage, the incomplete processing at intercistronic junctions is an alternative expression strategy for potyvirids, which deserve being paid more attention in future. Potyviral 6K1s are short in size (~54-aa), and 17 residues are rather conserved. It is so fascinating that 15 of them are essential for the successful infection of PVMV. Are these residues responsible for the functions of 6K1, P3-6K1, or both? To best define which residues are associated with biological significance of 6K1, these 6K1 variants with single alanine/arginine substitution of conserved residues are individually engineered into viral clone, and allowed for their expression along with viral infection, in order to interfere with the functions of inherent 6K1 in PVMV. Fortunately, four point mutants

532 interfere with viral infectivity, but also are associated with autophagic degradation of
533 6K1. In view of the limitations of this approach, it would be also possible that the
534 remaining conserved residues involve biological function of 6K1, could not be
535 precluded, or else, some residues are associated with the potential functions of P3-6K1.
536 For potyvirids, viral factors excluding P3N-PIPO are expressed through polyprotein
537 processing, and theoretically, should share an equivalent number of molecules during
538 viral infection. In fact, an extremely low abundance of 6K1 was observed in the context
539 of viral infection for all tested potyviruses (28, 30). In line with the observation, we
540 provide multi-disciplinary evidences in supporting a role of cellular autophagy on the
541 degradation of PVMV 6K1. Curiously, E-64d treatment increased the accumulation
542 level of 6K1, whereas 3-MA does not. The contrasting effects (3-MA versus E-64d
543 treatments) might be well explained by following facts: i) 3-MA is able to effectively
544 block an early stage of autophagy by inhibiting the formation of class III PI3K complex,
545 but does not inhibit Beclin1/VPS30/ATG6-independent autophagy pathways (66-68).
546 Beclin1 is a core component in the formation of autophagosomes. However, in
547 mammalian cells, it has been shown that several types of autophagy are induced in a
548 Beclin1/VPS30/ATG6-independent manner, and are not blocked by PI3K inhibitors (66,
549 69, 70). The formation of autophagosomes in this functional autophagy pathway just
550 need a subset of ATG proteins (66, 71). ii) Several studies showed that 3-MA might also
551 stimulate autophagy (72, 73), suggesting that it is not a preferable inhibitor for
552 autophagy-related research. iii) E-64d blocks the late steps of autophagy pathways
553 through inhibiting the activity of aspartic and cysteine proteases (74). Our finding

554 increases the possibility that Beclin1/VPS30/ATG6-independent autophagy pathway
555 might occur in plants.
556
557 **MATERIALS AND METHODS**
558 **Plant materials and virus source**
559 *N. benthamiana* and *C. chinense* (cultivar Yellow Lantern) plants were grown in a
560 growth chamber with the set of growth conditions as follows: 16-h light (6500 Lx) at
561 25°C and 8-h darkness at 23°C with the relative humidity of 70%. The infectious cDNA
562 clone of a PVMV isolate (PVMV-HNu), pHNu, was developed by our group (48), and
563 served as the backbone to produce a series of indicated recombinant and mutated viral
564 clones.
565 **Construction of PVMV-derived cDNA clones**
566 To create a GFP-tagged PVMV clone, the NIb/CP intercistronic junction in pHNu
567 (48) was subjected for the integration of a complete GFP-encoding sequence. The GFP
568 sequence was amplified from pVPH-GFP (30) with a pair of primers P-GFP-F/P-GFP-
569 R (Table S1). Another two regions, upstream and downstream of NIb/CP junction,
570 respectively, were amplified with corresponding primer sets C-F/C1-R and C2-F/C-R
571 (Table S1). A mixture of above obtained products was used as the template for
572 overlapping PCR with primer set C-F/C-R. The resulting fragment was inserted back
573 into pHNu (48) by utility of *Aat*II/*Sal*I sites to generate the recombinant clone, pHNu-
574 GFP.
575 To engineer a second copy of 6K1 into NIb/CP junction, the 6K1-coding sequence

was amplified by primer set NIb-6K1-F/6K1-CP-R (Table S1). Another two regions, upstream and downstream of NIb/CP junction, respectively, were amplified with corresponding primer sets C-F/NIb-6K1-R and 6K1-CP-F/C-R (Table S1). A mixture of the obtained PCR products was used as the template for overlapping PCR with the primer sets C-F/C-R. The resulting fragment was inserted into pHNu by utility of *Aat*II/*Sal*I sites to generate the clone pHNu//6K1. Using pHNu//6K1 as the backbone, a total of 15 mutated clones, i.e., pHNu//6K1(K3A), pHNu//6K1(E11A), pHNu//6K1(A15R), pHNu//6K1(L19A), pHNu//6K1(M22A), pHNu//6K1(D25A), pHNu//6K1(D27A), pHNu//6K1(R28A), pHNu//6K1(R30A), pHNu//6K1(V32A), pHNu//6K1(K34A), pHNu//6K1(L36A), pHNu//6K1(K38A), pHNu//6K1(L39A), and pHNu//6K1(K51A), were constructed for the generation of recombinant viruses with the mutation of corresponding conserved residues in the second copy of 6K1 into Ala or Arg. These clones were generated in the same strategy, and, herein, we described the construction of pHNu//6K1(K3A). Two primers K3A-F and K3A-R (Table S1) were synthesized, and, respectively, paired with C-R and C-F for PCR reactions with pHNu//6K1 as the template. A mixture of the obtained PCR products was used as the template for overlapping PCR with the primer sets C-F/C-R. The resulting fragment was inserted into pHNu//6K1 by utility of *Aat*II/*Sal*I sites to generate the clone pHNu//6K1(K3A).

To integrate a GFP-tagged 6K1 into NIb/CP junction, one upstream fragment of 6K1-CP junction in pHNu//6K1 was amplified using primer set C-F/6K1-GFP-R (Table S1), another downstream fragment of NIb-GFP junction in pHNu-GFP was amplified with

primer set 6K1-GFP-F/C-R (Table S1). Two PCR products were mixed, and served as the template for overlapping PCR with primer set C-F/C-R. The resulting fragment was inserted into pHNu by utility of *Aat*II/*Sal*I sites to generate pHNu//6K1-GFP. Using a similar cloning strategy for the generation of pHNu//6K1(K3A), the following mutated clones based on pHNu//6K1-GFP were generated: pHNu//6K1(D30A)-GFP, pHNu//6K1(V32A)-GFP, pHNu//6K1(K34A)-GFP, pHNu//6K1(L36A)-GFP, and pHNu//6K1(L39A)-GFP.

To C-terminally fuse a Myc epitope with 6K1 protein in PVMV, two PCR reactions with pHNu-GFP as the template were performed by using primer sets 2280-F/6K1^{Myc}-R and 6K1^{Myc}-F/4070-R, respectively (Table S1). The obtained products were mixed and served as the template for overlapping PCR with primer set 2280-F/4070-R. The resulting fragment was inserted back into pHNu-GFP by utility of *Bam*HI/*Stu*I sites to generate the clone, pHNu-GFP-6K1^{Myc}. pHNu-GFP-^{Myc}P3 was constructed by using a similar strategy with that of pHNu-GFP-6K1^{Myc}. To destroy the cleavage at P3-6K1 junction by NIa-Pro, five mutated clones, i.e., pHNu-GFP-^{Myc}P3(Q-H), pHNu-GFP-^{Myc}P3(A-K), pHNu-GFP-^{Myc}P3(QA-AQ), pHNu-GFP-^{Myc}P3(Q-A), and pHNu-GFP-^{Myc}P3(A-Q), were constructed with pHNu-GFP-^{Myc}P3 as the backbone using a similar cloning strategy. Here, we described the construction of pHNu-GFP-^{Myc}P3(Q-H). Two primers Q-H-F and Q-H-R (Table S1), for which the original nucleotides coding for Gln at P1 position were substituted for encoding His, were synthesized, and, respectively, paired with 4070-R and 2280-F (Table S1) for PCR reactions. A mixture of obtained products served as template for overlapping PCR with primer set 4070-R

and 2280-F. The resulting fragment was inserted back into pHNu-GFP-^{Myc}P3 by utility of *Bam*HI/*Stu*I sites. Similarly, a total of 17 point mutants of PVMV-GFP-^{Myc}P3, in which the conserved residues in 6K1 were substituted with Ala or Arg, were developed.

Generation of T-DNA constructs

A binary plant-expression vector - pCaMterX (75) was employed to transiently express genes of interest in *N. benthamiana*. The coding sequence of GFP and mCherry were amplified from pVPH-GFP//mCherry (30) using primer sets GFP-F/GFP-R and mCherry-F/ mCherry-R (Table S1), respectively. The resulting fragments were individually integrated into pCaMterX by utility of *Xba*I/*Bam*HI sites to generate the clones, pCaM-GFP and pCaM-mCherry. To develop the constructs for transiently expressing NbATG8a and NbATG8f whose N-termini were fused with mCherry, the coding sequences of NbATG8a and NbATG8f were amplified by using cDNAs prepared from *N.benthamiana* leaves with primer sets NbATG8a-Bam-F/NbATG8a-Kpn-R and NbATG8f-Bam-F/NbATG8f-Kpn-R (Table S1), respectively. The resulting PCR products were individually integrated into pCaM-mCherry by utility of *Bam*HI/*Kpn*I to generate the clones, pCaM-mCherry-NbATG8a and pCaM-mCherry-NbATG8f. The coding sequence of 6K2 was amplified from pHNu-GFP with a pair of primers 6K2-Xho-F/6K2-Xba-R (Table S1), the obtained PCR products were integrated into pCaM-mCherry by utility of *Xho*I/*Xba*I sites to generate the clone, pCaM-6K2-mCherry. Similarly, the construct pCaM-6K1-GFP for transiently expressing 6K1-GFP was generated. For the hairpin-mediated silencing in *N. benthamiana*, a partial sequence of coding region of *NbATG7* (324 nt) or β-glucuronidase gene (310 nt) was

642 cloned into p2300s-intron in both sense (*Sac*I/*Bam*HI) and antisense (*Pst*I/*Xba*I)
643 orientations.

644 All PCRs were performed with Phusion high-fidelity DNA polymerase (Thermo
645 Fisher Scientific), and all constructs were confirmed by sanger sequencing.

646 **Sequence analysis**

647 A total of 115 sequences of different potyviral 6K1s (Supplemental Data S1) were
648 retrieved from NCBI GenBank database, and subjected to multiple alignment. Multiple
649 alignment was performed using an online tool Clustal Omega
650 (https://www.ebi.ac.uk/Tools/msa/clustalo/) (76), followed by the description with the
651 online program Weblogo (http://weblogo.berkeley.edu/logo.cgi) (77, 78).

652 **Viral inoculation and agroinfiltration**

653 For infectivity test of PVMV-derived cDNA clones, agrobacterium (strain GV3101)
654 cultures harboring corresponding clones were suspended in infiltration buffer (10 mM
655 $MgCl_2$, 10 mM MES, and 150 μM acetosyringone), adjusted to OD_{600} of 1.0 and
656 infiltrated into fully expanded leaves of *N. benthamiana* seedlings at 6- to 8-leaf stage
657 or *C. chinense* plants at 3- to 4-leaf stage, unless otherwise stated. For subcellular
658 localization assays, agrobacterium (GV3101) culture harboring pHNu//6K1-GFP
659 (OD_{600}, 0.5), was mixed with another culture harboring either pCaM-mCherry-
660 NbATG8a or pCaM-mCherry-NbATG8f (OD_{600}, 0.5) in equal proportions, and co-
661 infiltrated into fully expanded leaves of *N. benthamiana* plants at 6- to 8-leaf stage.

662 To test whether 6K1 is colocalized with 6K2, fully expanded leaves of *N.*
663 *benthamiana* were firstly infiltrated with agrobacterial culture harboring pHNu//6K1-

GFP (OD600, 0.5). 24 h later, these patches were re-infiltrated with an agrobacterial culture harboring pCaM-6K2-mCherry (OD_{600}, 0.3). For hairpin-mediated silencing assays, each of agrobacterium cultures harboring pCaM-6K1-GFP or its mutants, together with another culture containing p2300s-intron-dsGUS or p2300s-intron-dsATG7, were adjusted to OD_{600} of 1.0, mixed with equal volumes, and co-infiltrated into fully expanded leaves of *N. benthamiana* plants at 6- to 8-leaf stage.

RNA analysis

Total RNAs were extracted from leaf tissues of *N. benthamiana* with TRNzol reagent (TIANGEN) and *C. chinense* with FastPure Plant Total RNA Isolation Kit (Vazyme). For RT-qPCR analysis, total RNAs (1 μg per sample) were treated with DNaseI (Thermo Fisher Scientific) following the manufacturer's instructions, followed by reverse-transcription with RevertAid First Strand cDNA Synthesis Kit (Thermo Fisher Scientific). The synthesized cDNAs were used to determine mRNA levels of target genes or quantification of viral accumulation levels. Specific primer pairs were designed using Primer3Plus (https://www.primer3plus.com/index.html) (79). qPCR was conducted by using SuperReal Premix Plus (TIANGEN) in Applied Biosystems QuantStudio 5 (Thermo Fisher Scientific). The transcripts of either *NbActin* or *CcActin* were selected as an internal control to normalize the data. Each experiment was performed at least three times, and the relative gene expression level were calculated by manufacturer's software.

Immunoblotting and antibodies

Total proteins were extracted from infiltrated leaf patches or systemically infected

686 leaves of *N. benthamiana* and *C. Chinense*, following a previously described protocal
687 (30). Immunoblotting assays were performed with anti-GFP rabbit polyclonal antibody
688 (BBI) or anti-Myc polyclonal antibody (Abcam) as the primary antiboty and
689 horseradish peroxidase (HRP)-conjugated goat anti-rabbit IgG (BBI) or goat anti-rabbit
690 immunoglobulin antibody (Abcam) as the secondary one, essentialy as described
691 previously (80). The immunological detection of target signals was performed using
692 enhanced chemiluminescence detection reagents (Thermo Fisher Scientific) in an
693 ImageQuant LAS 4000 mini biomolecular imager (GE Healthcare). The signal intensity
694 corresponding to protein bands was quantitatively analyzed with ImageJ software (81).

695 **Chemical treatments**

696 Fully expanded leaves of *N. benthamiana* plants, pre-inoculated with the indicated
697 plasmids, were treated with 1% DMSO in phosphate buffer (as the parallel control), or
698 an equal volume buffer containing 1% DMSO and 10 mM 3-MA, 100 μM E64d or 100
699 μM MG132 (Sigma). Sixteen hours after the treatment, leaf samples were collected for
700 immunoblotting analysis.

701 **Confocal microscopy**

702 The epidermal cells of infiltrated patches were examined by a confocal microscopy
703 (LSM 900, Zeiss) with a 20× dry immersion objective. Light emitted at 643 nm was
704 used to record chlorophyll auto-fluorescence; GFP was excited at 493 nm and captured
705 at 478-535 nm; mCherry was excited at 553 nm and captured at 548-629 nm. Images
706 were captured digitally and handled using Zeiss ZEN 3.7 software.

707 **Accession numbers in NCBI GenBank database**

PVMV-HNu (MN082715), *NbATG8a* (KX120976), *NbATG8f* (KU561372), *NbATG7* (KX369398), *CcActin* (AM168448).

ACKNOWLEDGMENTS

This work is supported by grants from the National Natural Science Foundation of China (31860487), and Collaborative Innovation Center of Nanfan and High-Efficiency Tropical Agriculture, Hainan University (XTCX2022NYB11). We would like to express our special appreciation to Dr. Yi Xu (Nanjing Agricultural University) for providing the plasmid p2300s-intron, and Dr. Wenping Qiu for critical reading.

H.C., W.H., Z.D., and X.X. conceived and designed the project. W.H., C.D., and L.Q. carried out experiments. H.C. supervised the work. All authors analyzed and discussed the data. H.C., and W.H. wrote the manuscript. All authors reviewed and approved the manuscript.

We declare no conflicts of interest.

REFERENCES

1. Revers F, García JA. 2015. Molecular biology of potyviruses. Adv Virus Res 92:101-99.

2. Cui H, Wang A. 2019. The biological impact of the hypervariable N-terminal region of potyviral genomes. Annu Rev Virol 6:255-274.

3. Yang X, Li Y, Wang A. 2021. Research advances in potyviruses: from the laboratory bench to the field. Annu Rev Phytopathol 59:1-29.

730 4. Pasin F, Daròs JA, Tzanetakis IE. 2022. Proteome expansion in the Potyviridae
731 evolutionary radiation. FEMS Microbiol Rev 46:fuac011.
732 5. Gibbs AJ, Hajizadeh M, Ohshima K, Jones RAC. 2020. The potyviruses: an
733 evolutionary synthesis is emerging. Viruses 12:132.
734 6. Mäkinen K, Aspelin W, Pollari M, Wang L. 2023. How do they do it? The infection
735 biology of potyviruses. Adv Virus Res 117:1-79.
736 7. Inoue-Nagata AK, Jordan R, Kreuze J, Li F, López-Moya JJ, Mäkinen K, Ohshima
737 K, Wylie SJ, Ictv Report Consortium. 2022. ICTV virus taxonomy profile: *Potyviridae*
738 2022. J Gen Virol 103.
739 8. Chung BY, Miller WA, Atkins JF, Firth AE. 2008. An overlapping essential gene in
740 the *Potyviridae*. Proc Natl Acad Sci U S A 105:5897-902.
741 9. Olspert A, Chung BY, Atkins JF, Carr JP, Firth AE. 2015. Transcriptional slippage in
742 the positive-sense RNA virus family *Potyviridae*. EMBO Rep 16:995-1004.
743 10. Rodamilans B, Valli A, Mingot A, San León D, Baulcombe D, López-Moya JJ,
744 García JA. 2015. RNA polymerase slippage as a mechanism for the production of
745 frameshift gene products in plant viruses of the *Potyviridae* family. J Virol 89:6965-7.
746 11. White KA. 2015. The polymerase slips and PIPO exists. EMBO Rep 16:885-6.
747 12. Mingot A, Valli A, Rodamilans B, San León D, Baulcombe DC, García JA, López-
748 Moya JJ. 2016. The P1N-PISPO trans-frame gene of sweet potato feathery mottle
749 potyvirus is produced during virus infection and functions as an RNA silencing
750 suppressor. J Virol 90:3543-57.

751 13. Untiveros M, Olspert A, Artola K, Firth AE, Kreuze JF, Valkonen JP. 2016. A novel
752 sweet potato potyvirus open reading frame (ORF) is expressed via polymerase slippage
753 and suppresses RNA silencing. Mol Plant Pathol 17:1111-23.
754 14. Gong P, Shen Q, Zhang M, Qiao R, Jiang J, Su L, Zhao S, Fu S, Ma Y, Ge L, Wang
755 Y, Lozano-Durán R, Wang A, Li F, Zhou X. 2023. Plant and animal positive-sense
756 single-stranded RNA viruses encode small proteins important for viral infection in their
757 negative-sense strand. Mol Plant 16:1794-1810.
758 15. Li F, Jia M, Wang A. 2024. Hidden viral proteins: how powerful are they? PLoS
759 Pathog 20:e1011905.
760 16. Cheng X, Wu X, Fang R. 2024. The minus strand of positive-sense RNA viruses
761 encodes small proteins. Trends Microbiol 32:6-7.
762 17. Martínez-Turiño S, García JA. 2020. Potyviral coat protein and genomic RNA: A
763 striking partnership leading virion assembly and more. Adv Virus Res 108:165-211.
764 18. Shen W, Shi Y, Dai Z, Wang A. 2020. The RNA-dependent RNA polymerase NIb
765 of potyviruses plays multifunctional, contrasting roles during viral infection. Viruses
766 12:77.
767 19. Restrepo-Hartwig MA, Carrington JC. 1994. The tobacco etch potyvirus 6-
768 kilodalton protein is membrane associated and involved in viral replication. J Virol
769 68:2388-97.
770 20. Schaad MC, Jensen PE, Carrington JC. 1997. Formation of plant RNA virus
771 replication complexes on membranes: role of an endoplasmic reticulum-targeted viral
772 protein. EMBO J 16:4049-59.

773 21. Wei T, Wang A. 2008. Biogenesis of cytoplasmic membranous vesicles for plant
774 potyvirus replication occurs at endoplasmic reticulum exit sites in a COPI- and COPII-
775 dependent manner. J Virol 82:12252-64.
776 22. Cotton S, Grangeon R, Thivierge K, Mathieu I, Ide C, Wei T, Wang A, Laliberté JF.
777 2009. Turnip mosaic virus RNA replication complex vesicles are mobile, align with
778 microfilaments, and are each derived from a single viral genome. J Virol 83:10460-71.
779 23. Wei T, Huang TS, McNeil J, Laliberté JF, Hong J, Nelson RS, Wang A. 2010.
780 Sequential recruitment of the endoplasmic reticulum and chloroplasts for plant
781 potyvirus replication. J Virol 84:799-809.
782 24. Rodríguez-Cerezo E, Shaw JG. 1991. Two newly detected nonstructural viral
783 proteins in potyvirus-infected cells. Virology 185:572-9.
784 25. García JA, Martín MT, Cervera MT, Riechmann JL. 1992. Proteolytic processing
785 of the plum pox potyvirus polyprotein by the NIa protease at a novel cleavage site.
786 Virology 188:697-703.
787 26. Riechmann JL, Cervera MT, García JA. 1995. Processing of the plum pox virus
788 polyprotein at the P3-6K1 junction is not required for virus viability. J Gen Virol
789 76:951-6.
790 27. Merits, A., Rajamäki, M. L., Lindholm, P., Runeberg-Roos, P., Kekarainen, T.,
791 Merits A, Rajamäki ML, Lindholm P, Runeberg-Roos P, Kekarainen T, Puustinen P,
792 Mäkeläinen K, Valkonen JPT, Saarma M. 2002. Proteolytic processing of potyviral
793 proteins and polyprotein processing intermediates in insect and plant cells. J Gen Virol
794 83:1211-1221.

795 28. Waltermann A, Maiss E. 2006. Detection of 6K1 as a mature protein of 6 kDa in
796 plum pox virus-infected *Nicotiana benthamiana*. J Gen Virol 87:2381-2386.
797 29. Kekarainen T, Savilahti H, Valkonen JP. 2002. Functional genomics on potato virus
798 A: virus genome-wide map of sites essential for virus propagation. Genome Res
799 12:584-94.
800 30. Cui H, Wang A. 2016. Plum pox virus 6K1 protein is required for viral replication
801 and targets the viral replication complex at the early stage of infection. J Virol 90:5119-
802 5131.
803 31. Geng C, Yan ZY, Cheng DJ, Liu J, Tian YP, Zhu CX, Wang HY, Li XD. 2017.
804 Tobacco vein banding mosaic virus 6K2 protein hijacks NbPsbO1 for virus replication.
805 Sci Rep 7:43455.
806 32. Fang L, Geng C, Wei XY, Dong CC, Pang JP, Yan ZY, Jiang J, Tian YP, Li XD.
807 2024. Potato virus Y viral protein 6K1 inhibits the interaction between defense proteins
808 during virus infection. Plant Physiol 194:1447-1466.
809 33. Liu Y, Bassham DC. 2012. Autophagy: pathways for self-eating in plant cells. Annu
810 Rev Plant Biol 63:215-37.
811 34. Marshall RS, Vierstra RD. 2018. Autophagy: the master of bulk and selective
812 recycling. Annu Rev Plant Biol 69:173-208.
813 35. Yu L, Chen Y, Tooze SA. 2018. Autophagy pathway: cellular and molecular
814 mechanisms. Autophagy 14:207-215.
815 36. Clavel M, Michaeli S, Genschik P. 2017. Autophagy: a double-edged sword to fight
816 plant viruses. Trends Plant Sci 22:646-648.

817 37. Kushwaha NK, Hafrén A, Hofius D. 2019. Autophagy-virus interplay in plants:
818 from antiviral recognition to proviral manipulation. Mol Plant Pathol 20:1211-1216.
819 38. Yang M, Ismayil A, Liu Y. 2020. Autophagy in Plant-Virus Interactions. Annu Rev
820 Virol 7:403-419.
821 39. Valli AA, Gallo A, Rodamilans B, López-Moya JJ, García JA. 2018. The HCPro
822 from the *Potyviridae* family: an enviable multitasking helper component that every
823 virus would like to have. Mol Plant Pathol 19:744-763.
824 40. Nakahara KS, Masuta C, Yamada S, Shimura H, Kashihara Y, Wada TS, Meguro A,
825 Goto K, Tadamura K, Sueda K, Sekiguchi T, Shao J, Itchoda N, Matsumura T, Igarashi
826 M, Ito K, Carthew RW, Uyeda I. 2012. Tobacco calmodulin-like protein provides
827 secondary defense by binding to and directing degradation of virus RNA silencing
828 suppressors. Proc Natl Acad Sci U S A 109:10113-8.
829 41. Hafrén A, Üstün S, Hochmuth A, Svenning S, Johansen T, Hofius D. 2018. Turnip
830 mosaic virus counteracts selective autophagy of the viral silencing suppressor HCpro.
831 Plant Physiol 176:649-662.
832 42. Li F, Zhang C, Li Y, Wu G, Hou X, Zhou X, Wang A. 2018. Beclin1 restricts RNA
833 virus infection in plants through suppression and degradation of the viral polymerase.
834 Nat Commun 9:1268.
835 43. Cheng X, Wang A. 2016. The potyvirus silencing suppressor protein VPg mediates
836 degradation of SGS3 via ubiquitination and autophagy pathways. J Virol 91: e01478-
837 16.

838 44. Cheng G, Yang Z, Zhang H, Zhang J, Xu J. 2020. Remorin interacting with PCaP1
839 impairs turnip mosaic virus intercellular movement but is antagonised by VPg. New
840 Phytol 225:2122-2139.
841 45. Li F, Zhang C, Tang Z, Zhang L, Dai Z, Lyu S, Li Y, Hou X, Bernards M, Wang A.
842 2020. A plant RNA virus activates selective autophagy in a UPR-dependent manner to
843 promote virus infection. New Phytol 228:622-639.
844 46. Ji M, Zhao J, Han K, Cui W, Wu X, Chen B, Lu Y, Peng J, Zheng H, Rao S, Wu G,
845 Chen J, Yan F. 2021. Turnip mosaic virus P1 suppresses JA biosynthesis by degrading
846 cpSRP54 that delivers AOCs onto the thylakoid membrane to facilitate viral infection.
847 PLoS Pathog 17:e1010108.
848 47. Majer E, Salvador Z, Zwart MP, Willemsen A, Elena SF, Daròs JA. 2014.
849 Relocation of the NIb gene in the tobacco etch potyvirus genome. J Virol 88:4586-90.
850 48. Hu W, Qin L, Yan H, Miao W, Cui H, Liu W. 2020. Use of an infectious cDNA
851 clone of pepper veinal mottle virus to confirm the etiology of a disease in *Capsicum*
852 *chinense*. Phytopathology 110:80-84.
853 49. Adams MJ, Antoniw JF, Beaudoin F. 2005. Overview and analysis of the
854 polyprotein cleavage sites in the family *Potyviridae*. Mol Plant Pathol 6:471-487.
855 50. Dougherty WG, Carrington JC, Cary SM, Parks TD. 1988. Biochemical and
856 mutational analysis of a plant virus polyprotein cleavage site. EMBO J 7:1281-7.
857 51. Kapust RB, Tözsér J, Copeland TD, Waugh DS. 2002. The P1' specificity of tobacco
858 etch virus protease. Biochem Biophys Res Commun 294:949-55.

859 52. Jiang J, Patarroyo C, Garcia Cabanillas D, Zheng H, Laliberté JF. 2015. The vesicle-
860 forming 6K2 protein of turnip mosaic virus interacts with the COPII coatomer Sec24a
861 for viral systemic infection. J Virol 89:6695-710.
862 53. Hu T, Luan H, Wang L, Ren R, Sun L, Yin J, Liu H, Jin T, Li B, Li K, Zhi H. 2023.
863 Soybean mosaic virus 6K1 interactors screening and GmPR4 and GmBI1 function
864 characterization. Int J Mol Sci 24:5304.
865 54. Klionsky DJ, Emr SD. 2000. Autophagy as a regulated pathway of cellular
866 degradation. Science 290:1717-21.
867 55. Smalle J, Vierstra RD. 2004. The ubiquitin 26S proteasome proteolytic pathway.
868 Annu Rev Plant Biol 55:555-90.
869 56. Haxim Y, Ismayil A, Jia Q, Wang Y, Zheng X, Chen T, Qian L, Liu N, Wang Y, Han
870 S, Cheng J, Qi Y, Hong Y, Liu Y. 2017. Autophagy functions as an antiviral mechanism
871 against geminiviruses in plants. Elife 6:e23897.
872 57. Tong X, Liu SY, Zou JZ, Zhao JJ, Zhu FF, Chai LX, Wang Y, Han C, Wang XB.
873 2021. A small peptide inhibits siRNA amplification in plants by mediating autophagic
874 degradation of SGS3/RDR6 bodies. EMBO J 40:e108050.
875 58. Chai M, Li L, Li Y, Yang Y, Wang Y, Jiang X, Luan Y, Li F, Cui H, Wang A, Xiang
876 W, Wu X, Cheng X. 2024. The 6-kilodalton peptide 1 in plant viruses of the family
877 Potyviridae is a viroporin. Proc Natl Acad Sci U S A (accepted).
878 59. Bera S, Arena GD, Ray S, Flannigan S, Casteel CL. 2022. The Potyviral Protein
879 6K1 Reduces Plant Proteases Activity during Turnip mosaic virus Infection. Viruses
880 14:1341.

881 60. Bar-Ziv A, Levy Y, Hak H, Mett A, Belausov E, Citovsky V, Gafni Y. 2012. The
882 tomato yellow leaf curl virus (TYLCV) V2 protein interacts with the host papain-like
883 cysteine protease CYP1. Plant Signal Behav 7:983-9.
884 61. Bar-Ziv A, Levy Y, Citovsky V, Gafni Y. 2015. The tomato yellow leaf curl virus
885 (TYLCV) V2 protein inhibits enzymatic activity of the host papain-like cysteine
886 protease CYP1. Biochem Biophys Res Commun 460:525-529.
887 62. Misas-Villamil JC, van der Hoorn RA, Doehlemann G. 2016. Papain-like cysteine
888 proteases as hubs in plant immunity. New Phytol 212:902-907.
889 63. Liu P, Shi C, Liu S, Lei J, Lu Q, Hu H, Ren Y, Zhang N, Sun C, Chen L, Jiang Y,
890 Feng L, Zhang T, Zhong K, Liu J, Zhang J, Zhang Z, Sun B, Chen J, Tang Y, Chen F,
891 Yang J. 2023. A papain-like cysteine protease-released small signal peptide confers
892 wheat resistance to wheat yellow mosaic virus. Nat Commun 14:7773.
893 64. Carrington JC, Freed DD, Sanders TC. 1989. Autocatalytic processing of the
894 potyvirus helper component proteinase in Escherichia coli and in vitro. J Virol 63:4459-
895 63.
896 65. Kasschau KD, Carrington JC. 1995. Requirement for HC-Pro processing during
897 genome amplification of tobacco etch potyvirus. Virology 209:268-73.
898 66. Zhu JH, Horbinski C, Guo F, Watkins S, Uchiyama Y, Chu CT. 2007. Regulation of
899 autophagy by extracellular signal-regulated protein kinases during 1-methyl-4-
900 phenylpyridinium-induced cell death. Am J Pathol 170:75-86.
901 67. Michiorri S, Gelmetti V, Giarda E, Lombardi F, Romano F, Marongiu R, Nerini-
902 Molteni S, Sale P, Vago R, Arena G, Torosantucci L, Cassina L, Russo MA,

903 Dallapiccola B, Valente EM, Casari G. 2010. The Parkinson-associated protein PINK1
904 interacts with Beclin1 and promotes autophagy. Cell Death Differ 17:962-74.
905 68. Klionsky DJ, Abdel-Aziz AK, Abdelfatah S, Abdellatif M, Abdoli A, Abel S,
906 Abeliovich H, Abildgaard MH, Abudu YP, Acevedo-Arozena A, Adamopoulos IE,
907 Adeli K, Adolph TE, Adornetto A, Aflaki E, Agam G, Agarwal A, Aggarwal BB,
908 Agnello M, Agostinis P, … Tong CK. 2021. Guidelines for the use and interpretation of
909 assays for monitoring autophagy (4th edition). Autophagy 17:1-382.
910 69. Scarlatti F, Maffei R, Beau I, Codogno P, Ghidoni R. 2008. Role of non-canonical
911 Beclin 1-independent autophagy in cell death induced by resveratrol in human breast
912 cancer cells. Cell Death Differ 15:1318-29.
913 70. Sok SP, Arshad NM, Azmi MN, Awang K, Ozpolat B, Hasima Nagoor N. 2017. The
914 apoptotic effect of 1'S-1'-Acetoxychavicol Acetate (ACA) enhanced by inhibition of
915 non-canonical autophagy in human non-small cell lung cancer cells. PLoS One
916 12:e0171329.
917 71. Scarlatti F, Maffei R, Beau I, Ghidoni R, Codogno P. 2008. Non-canonical
918 autophagy: an exception or an underestimated form of autophagy? Autophagy 4:1083-
919 5.
920 72. Wu, Y. T., Tan, H. L., Shui, G., Bauvy, C., Huang, Q., Wenk, M. R., Ong, C. N., Wu
921 YT, Tan HL, Shui G, Bauvy C, Huang Q, Wenk MR, Ong CN, Codogno P, Shen HM.
922 2010. Dual role of 3-methyladenine in modulation of autophagy via different temporal
923 patterns of inhibition on class I and III phosphoinositide 3-kinase. J Biol Chem
924 285:10850-61.

925 73. Dembitz V, Lalic H, Visnjic D. 2017. 5-Aminoimidazole-4-carboxamide
926 ribonucleoside-induced autophagy flux during differentiation of monocytic leukemia
927 cells. Cell Death Discov 3:17066.
928 74. Moriyasu Y, Inoue Y. 2008. Use of protease inhibitors for detecting autophagy in
929 plants. Methods Enzymol 451:557-80.
930 75. Joensuu JJ, Conley AJ, Lienemann M, Brandle JE, Linder MB, Menassa R. 2010.
931 Hydrophobin fusions for high-level transient protein expression and purification in
932 *Nicotiana benthamiana*. Plant Physiol 152:622-33.
933 76. Madeira F, Pearce M, Tivey ARN, Basutkar P, Lee J, Edbali O, Madhusoodanan N,
934 Kolesnikov A, Lopez R. 2022. Search and sequence analysis tools services from
935 EMBL-EBI in 2022. Nucleic Acids Res 50:W276-W279.
936 77. Schneider TD, Stephens RM. 1990. Sequence logos: a new way to display
937 consensus sequences. Nucleic Acids Res 18:6097-100.
938 78. Crooks GE, Hon G, Chandonia JM, Brenner SE. 2004. WebLogo: a sequence logo
939 generator. Genome Res 14:1188-90.
940 79. Untergasser A, Cutcutache I, Koressaar T, Ye J, Faircloth BC, Remm M, Rozen SG.
941 2012. Primer3--new capabilities and interfaces. Nucleic Acids Res 40:e115.
942 80. Hu W, Dai Z, Liu P, Deng C, Shen W, Li Z, Cui H. 2023b. The single distinct leader
943 protease encoded by alpinia oxyphylla mosaic virus (Genus *Macluravirus*) suppresses
944 RNA silencing through interfering with double-stranded RNA synthesis.
945 Phytopathology 113:1103-1114.

946 81. Schneider CA, Rasband WS, Eliceiri KW. 2012. NIH Image to ImageJ: 25 years of
947 image analysis. Nat Methods 9:671-5.

948

949 **FIGURE LEGENDS**

950 **Fig. 1 Infectivity test of pHNu-GFP in *N. benthamiana* and *C. chinense*.** (A) A
951 schematic diagram of GFP-tagged PVMV clone (pHNu-GFP). A complete GFP-coding
952 sequence was engineered into NIb/CP junction of pHNu (48) to produce the
953 recombinant clone pHNu-GFP. For pHNu-GFP, the original cleavage site
954 'DFVLHQ/AG' at NIb/CP junction was respectively integrated into NIb/GFP and
955 GFP/CP junctions. The mutated nucleotides (in red) without altering cleavage peptide
956 sequence were introduced to avoid the removal of *GFP* sequence via recombination
957 event during viral replication. (B) Infectivity test of pHNu-GFP in *N. benthamiana*. The
958 representative plants were photographed under UV lamp. Mock, empty vector control,
959 pCB301. The close-view of indicated regions by rectangles is shown. (C) Infectivity
960 test of pHNu-GFP in *C. chinense*. (D) Immunoblotting detection of free GFP in top
961 non-inoculated leaves of *N. benthamiana* and *C. chinense* plants. The bands indicated
962 by asterisks correspond to the predicted size of free GFP (~27.7 kDa). A Coomassie
963 brilliant blue-stained gel was used as a loading control. Two samples per treatment were
964 assayed.

965 **Fig. 2 The effects of 17 different point substitutions in PVMV 6K1 on viral**
966 **infectivity in both *N. benthamiana* and *C. chinense*.** (A) The analysis of amino acid
967 conservation of 115 sequences of 6K1 from different potyviruses. The order of amino

968 acids was sorted with reference to PVMV 6K1. Alkaline amino acids are shown in blue,
969 acidic ones in red, and the rest in black. (B, D) Infectivity test of mutated PVMV clones
970 in *N. benthamiana* (B) and *C. chinense* (D). A close-view of representative plants is
971 shown. The GFP signals were examined under an handheld UV lamp in a darkness
972 room at the indicated time points. (C, E) Sequencing analysis of virus progeny.
973 Sequence comparison across WT, mutated clones, and viral progeny. The mutated sites
974 and surrounding sequences are shown. The sequences of viral progeny derived from
975 WT(V32A) and WT(K40A) in *N. benthamiana* was determined at 19 dpi (C). The
976 sequences of viral progeny derived from WT(V32A) and WT(A15R) in *C. chinense*
977 were determined at 25 dpi. The amino acids corresponding to the codons are shown in
978 blue, and reversion and compensatory mutations are shaded in red. (F) Summary on the
979 infectivity of different mutated clones in *N. benthamiana* and *C. chinense*. √, the
980 mutated clones that are able to efficiently infect plants; ×, the clones that are disabled
981 in successful infection; σ, the clones that are attenuated in systemic infection.

982 **Fig. 3 The expression profile of 6K1 during PVMV infection.** (A) Schematic
983 diagrams of pHNu-GFP-^{Myc}P3 and pHNu-GFP-6K1^{Myc}. The dotted line in red denotes
984 the self-cleavage site of HCPro, and the white ones represent the cleavage sites by NIa-
985 Pro. (B) Infectivity test of pHNu-GFP-^{Myc}P3 and pHNu-GFP-6K1^{Myc}. The GFP signals
986 in inoculated *N. benthamiana* plants are examined under a handheld UV lamp at 8 dpi.
987 The close-up of leaves in white rectangle are shown. Mock, empty vector control. (C)
988 RT-PCR detection of viral infection in inoculated plants. The upper non-inoculated
989 leaves were sampled at 8 dpi for RT-PCR detection with primer set PVMV-F/PVMV-R

(48) targeting viral *CP* cistron. (D) Sequencing analysis of virus progeny derived from pHNu-GFP-6K1^{Myc} and pHNu-GFP-^{Myc}P3. The upper non-inoculated leaves were harvested at 8 dpi, and used for cloning and sequencing. (E) Immunoblot detection of the expression profile of 6K1 in viral infection. I.L., inoculated leaves; T.L., upper non-inoculated leaves. Immunoblot analysis of the sample from upper non-inoculated leaves of pHNu-GFP at 8 dpi was included as the negative control. A Coomassie brilliant blue-stained gel was used as a loading control. (F) Immunoblotting analysis of the expression of ^{Myc}P3 and ^{Myc}P3-6K1 in viral infection. The upper non-inoculated leaves were sampled for the assay at the indicated time points. Immunoblot analysis of the sample from upper non-inoculated leaves of pHNu-GFP at 8 dpi was included as the negative control. A Coomassie brilliant blue-stained of Rubiso large unit (RbCL) was used as a loading control.

Fig. 4 Proteolytic processing at P3-6K1 junction by NIa-Pro is indispensable for the successful infection of PVMV. (A) Schematic diagram showing the mutations introduced into conserved heptapeptide at P3-6K1 junction. NIa-Pro cleavage site between P3 and 6K1 is indicated by a red arrow. The amino acids of heptapeptide were positioned as P1 through P6 and P1′, with reference to a previous document (49). The introduced mutated amino acids are shown in red. (B, C) The effects of different mutations at the cleavage site between P3 and 6K1 on viral infectivity in *N. benthamiana*. Representative plants were photographed at 8 dpi (B) or 30 dpi (C). The GFP signals in each representative plant were examined under a handheld UV lamp in a darkness room. The leaf regions in yellow rectangle are enlarged. Mock, empty vector

control. (D, E) Immunoblotting analysis of the expression of P3 and P3-6K1. Leaf patches inoculated with the indicated clones were sampled at 5 dpi, and were used for immunoblot detection of P3 and P3-6K1 by using an anti-Myc polyclonal antibody. A Coomassie brilliant blue-stained gel was used as a loading control.

Fig. 5 PVMV 6K1 is degraded by cellular autophagy. (A) Schematic diagram of pHNu//6K1-GFP. The red lines flanking 6K1-GFP represent NIa-Pro's cleavage sites at NIb-6K1-GFP and 6K1-GFP-CP junctions. (B) The patch design for the combinations of agrobacterial infiltration and chemical inhibitor treatment in the same leaves. 1 st, primary infiltration with agrobacterial culture harboring pHNu-GFP or pHNu//6K1-GFP; 2 nd, treatment with chemical inhibitor or DMSO. (C) The effects of ubiquitin-proteasome and autophagy pathways on the degradation of 6K1 in the context of viral infection. The signal intensity of protein bands is shown above the panel. The value for the combination of pHNu//6K1-GFP and p2300s-intron-dsGUS is designated as 1.0 to normalize the data. A Coomassie brilliant blue-stained gel was used as a loading control. (D) Co-localization of 6K1-GFP and 6K2-mCherry in the context of viral infection. Arrows, overlapped structures of 6K1-GFP and 6K2-mCherry. Bar, 50 μm. (E) Co-localization of 6K1-GFP and mCherry-NbATG8a or mCherry-NbATG8f at 60 hpi. Arrows, overlapped structures of 6K1-GFP and mCherry-NbATG8a / mCherry-NbATG8f. Bars, 50 μm. (F) The patch design for co-infiltration with agrobacterial cultures harboring pCaM-6K1-GFP and p2300s-intron-dsATG7 / p2300s-intron-dsGUS. (G) RT-qPCR analysis of the abundance of *NbATG7* mRNA transcripts at 3 dpi. The expression level of *NbActin* transcripts was determined to normalize the data. Error

bars denote standard errors from three biological replicates. Statistically significant differences, determined by an unpaired two-tailed Student's *t* test, are indicated by asterisks: **, 0.001<*P*< 0.01. (H) Effect of *NbATG7* knockdown on the accumulation of 6K1-GFP. Western blot analysis of the abundance of 6K1-GFP at 3 dpi. A Coomassie brilliant blue-stained gel was used as a loading control.

Fig. 6 Individual expression of five 6K1 mutants along with viral infection delays the infection progression in both *N. benthamiana* and *C. chinense*. (A) Schematic diagram of pHNu//6K1 and pHNu//6K1 variants. (B, D) Infectivity test of pHNu//6K1 variants in both *N. benthamiana* and *C. chinense*. Photographs were taken at 5 dpi for *N. benthamiana* (B), and at 10 dpi for *C. chinense* (D). (C, E) RT-qPCR analysis of viral accumulation levels. The upper non-inoculated leaves of *N. benthamiana* at 5 dpi (C) and *C. chinense* at 10 dpi (E), were sampled for RT-qPCR assays. The expression levels of *NbActin* and its ortholog in *C. chinense* (*CcActin*) transcripts were determined to normalize the data. Error bars denote standard errors from three biological replicates. Statistically significant differences, determined by an unpaired two-tailed Student's *t* test, are indicated by asterisk: **, 0.001<*P*< 0.01; *, 0.01<*P*< 0.05.

Fig. 7 Alanine substitutions of conserved residues (V32, K34, L36, L39) encompassed in a lysine/arginine-rich motif in 6K1 inhibited its autophagic degradation. (A) Schematic diagram of pHNu//6K1 variants-GFP. (B) The patch design for the combinations of agrobacterial infiltration and chemical inhibitor treatment in the same leaves. 1 st, primary infiltration with agrobacterial culture harboring pHNu//6K1-GFP or pHNu//6K1 variants-GFP; 2 nd, treatment with E-64d or

DMSO. (C) The effects of E-64d treatment on the accumulation of 6K1 variants in the context of viral infection. The signal intensity of protein bands is shown above the panel. The values for DMSO treatment were designated as 1.0 to normalize the data. -, DMSO treatment; +, E-64d treatment. Coomassie brilliant blue-stained gels were used as loading controls. (D) The patch design for co-infiltration with agrobacterial cultures harboring pCaM-6K1-GFP / pCaM-6K1(point mutaion)-GFP and p2300s-intron-dsATG7 / p2300s-intron-dsGUS. (E) Effect of *NbATG7* knockdown on the accumulation of 6K1-GFP or 6K1 variants-GFP. Western blot analysis of the abundance of 6K1-GFP or 6K1 variants-GFP at 3 dpi. Coomassie brilliant blue-stained gels were used as loading controls.

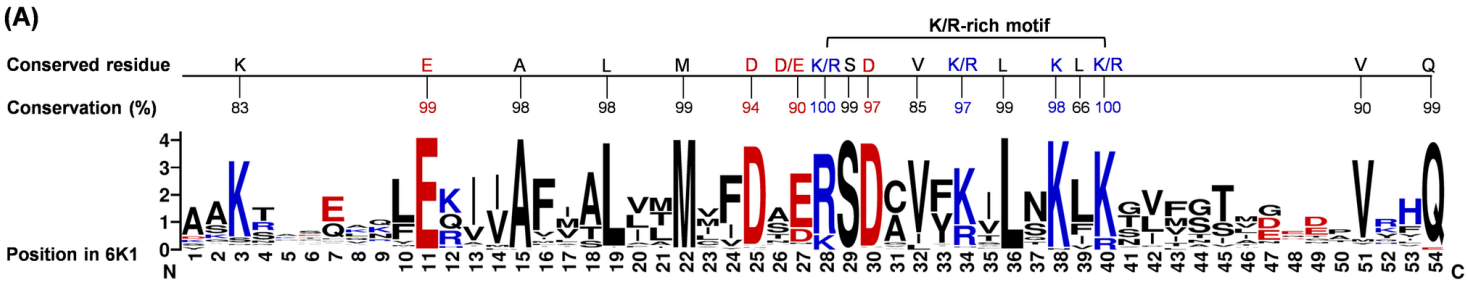

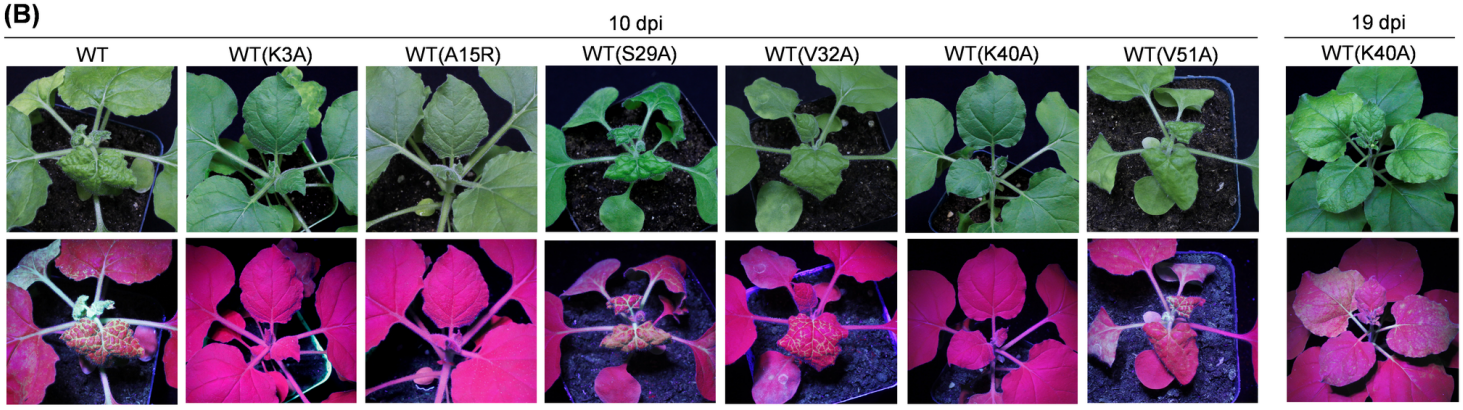

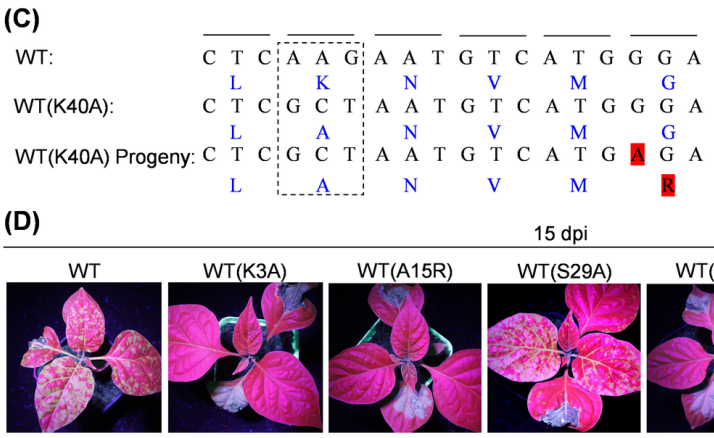

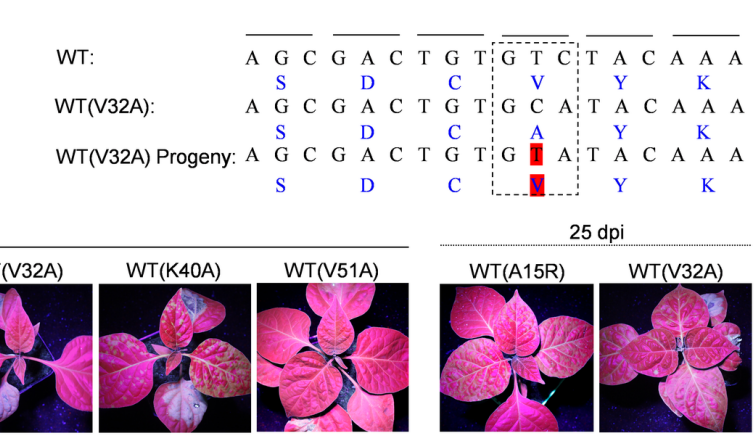

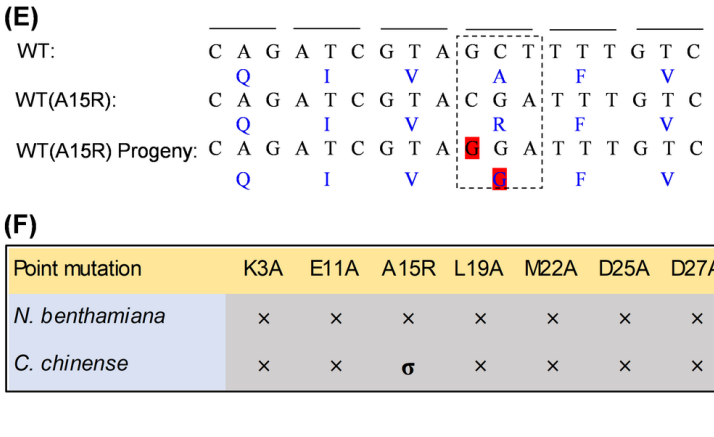

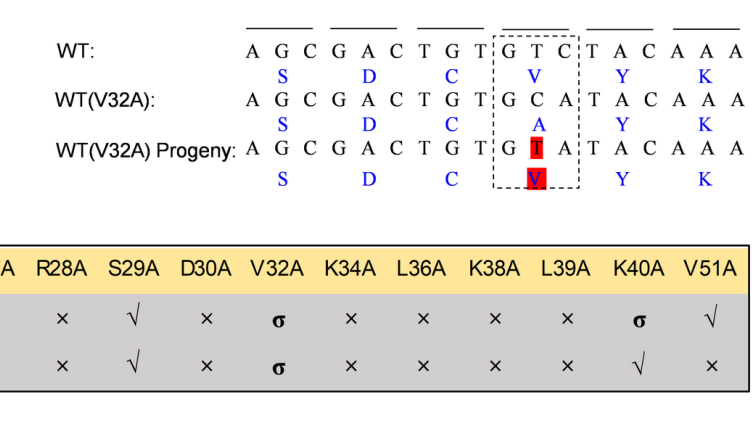

(F)

Point mutation	K3A	E11A	A15R	L19A	M22A	D25A	D27A	R28A	S29A	D30A	V32A	K34A	L36A	K38A	L39A	K40A	V51A
N. benthamiana	×	×	×	×	×	×	×	×	√	×	σ	×	×	×	×	σ	√
C. chinense	×	×	σ	×	×	×	×	×	√	×	σ	×	×	×	×	√	×

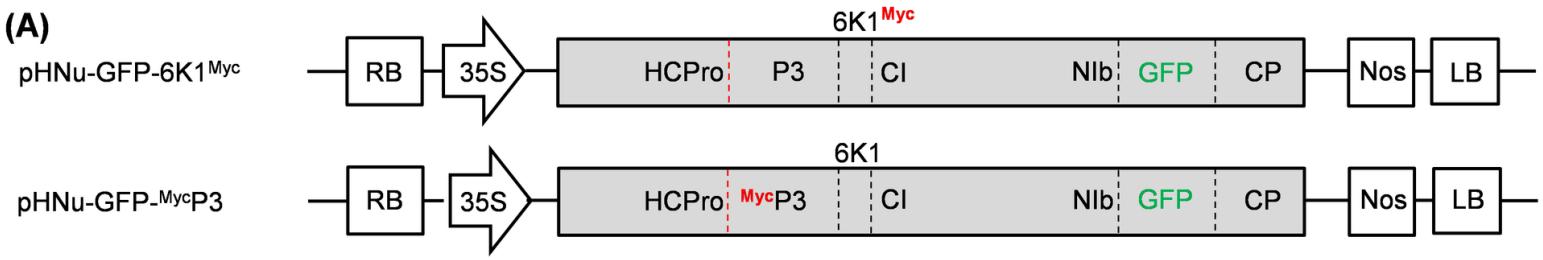
(A)
pHNu-GFP-6K1Myc
RB
35S
6K1Myc
HCPro
P3
CI
NIb
GFP
CP
Nos
LB
pHNu-GFP-MycP3
6K1
MycP3

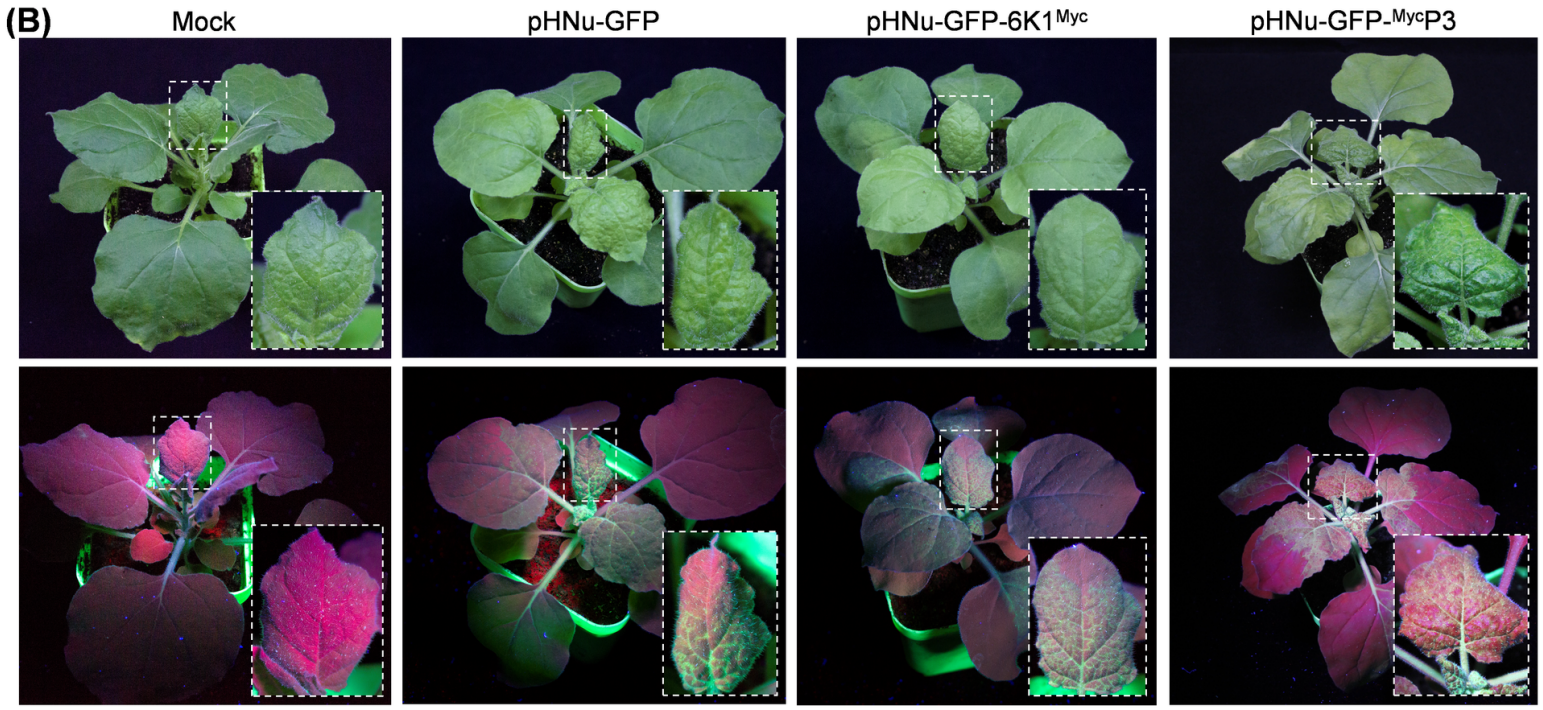
(B)
Mock
pHNu-GFP
pHNu-GFP-6K1Myc
pHNu-GFP-MycP3

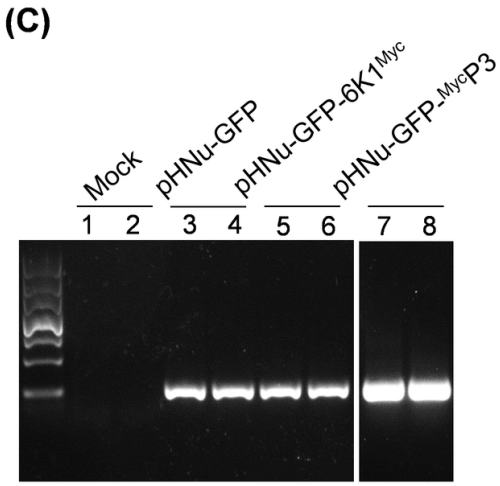
(C)
Mock
pHNu-GFP
pHNu-GFP-6K1Myc
pHNu-GFP-MycP3
1 2 3 4 5 6 7 8

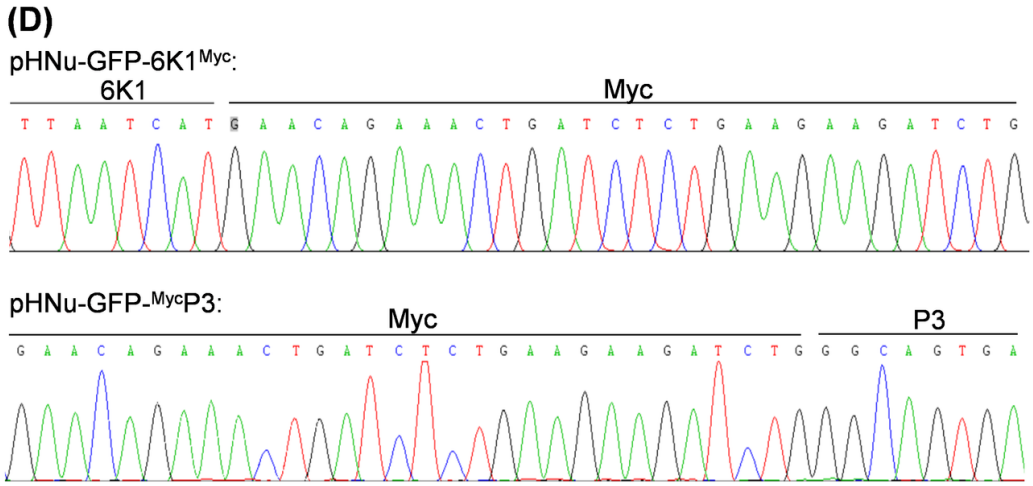
(D)
pHNu-GFP-6K1Myc:
6K1
Myc
pHNu-GFP-MycP3:
Myc
P3

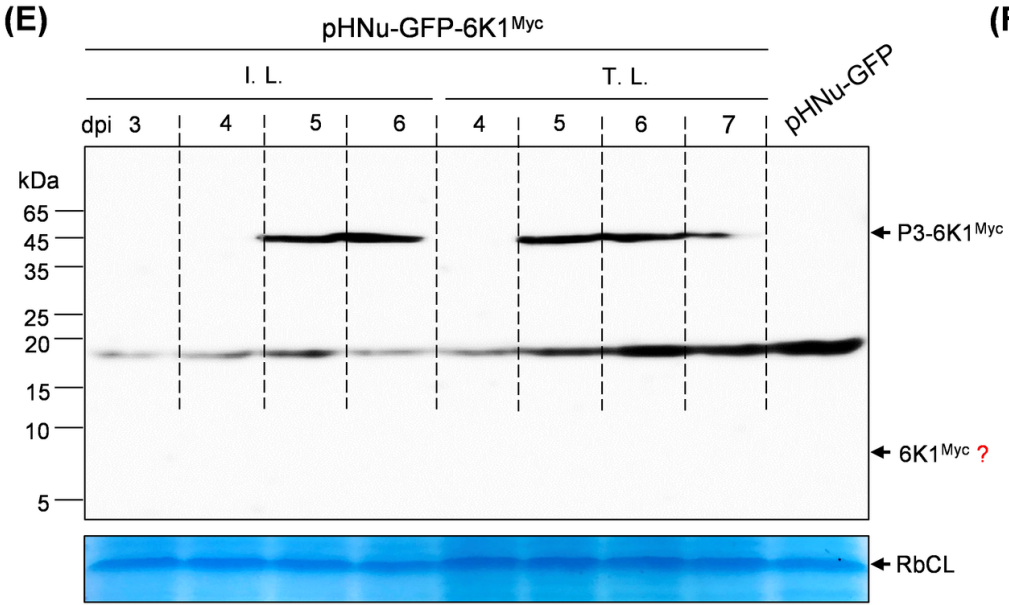
(E)
pHNu-GFP-6K1Myc
I. L.
T. L.
pHNu-GFP
dpi 3 4 5 6 4 5 6 7
kDa
65
45
35
25
20
15
10
5
P3-6K1Myc
6K1Myc ?
RbCL

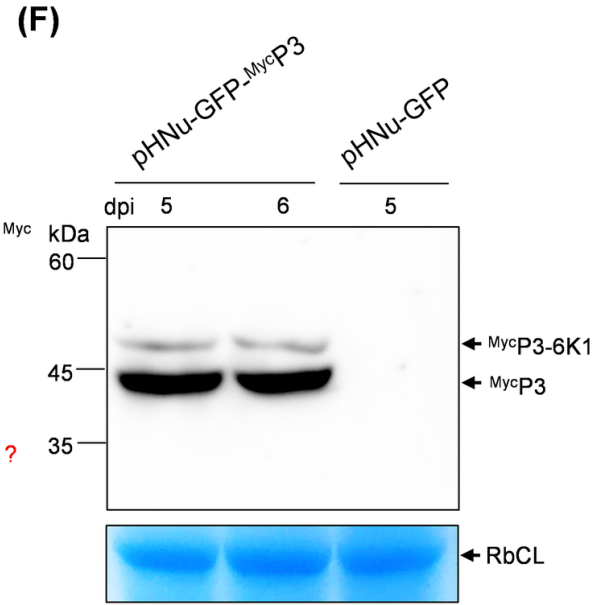
(F)
pHNu-GFP-MycP3
pHNu-GFP
dpi 5 6 5
kDa
60
45
35
MycP3-6K1
MycP3
RbCL

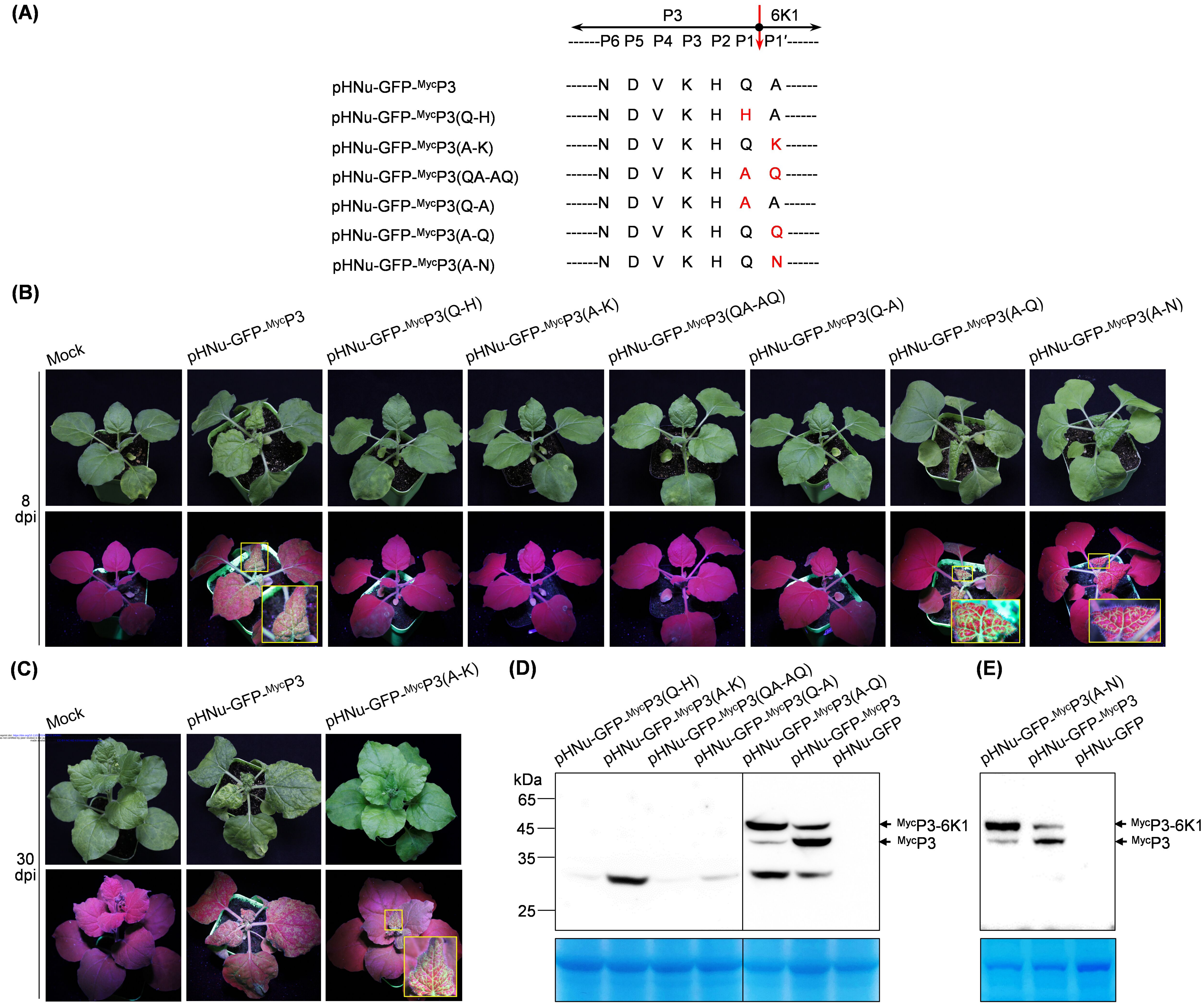
(A)
P3
6K1
------P6 P5 P4 P3 P2 P1 P1′------
pHNu-GFP-MycP3 ------N D V K H Q A ------
pHNu-GFP-MycP3(Q-H) ------N D V K H H A ------
pHNu-GFP-MycP3(A-K) ------N D V K H Q K ------
pHNu-GFP-MycP3(QA-AQ) ------N D V K H A Q ------
pHNu-GFP-MycP3(Q-A) ------N D V K H A A ------
pHNu-GFP-MycP3(A-Q) ------N D V K H Q Q ------
pHNu-GFP-MycP3(A-N) ------N D V K H Q N ------
(B)
Mock
pHNu-GFP-MycP3
pHNu-GFP-MycP3(Q-H)
pHNu-GFP-MycP3(A-K)
pHNu-GFP-MycP3(QA-AQ)
pHNu-GFP-MycP3(Q-A)
pHNu-GFP-MycP3(A-Q)
pHNu-GFP-MycP3(A-N)
8 dpi
(C)
Mock
pHNu-GFP-MycP3
pHNu-GFP-MycP3(A-K)
30 dpi
(D)
pHNu-GFP-MycP3(Q-H)
pHNu-GFP-MycP3(A-K)
pHNu-GFP-MycP3(QA-AQ)
pHNu-GFP-MycP3(Q-A)
pHNu-GFP-MycP3(A-Q)
pHNu-GFP-MycP3
pHNu-GFP
kDa
65
45
35
25
MycP3-6K1
MycP3
(E)
pHNu-GFP-MycP3(A-N)
pHNu-GFP-MycP3
pHNu-GFP
MycP3-6K1
MycP3

(A)

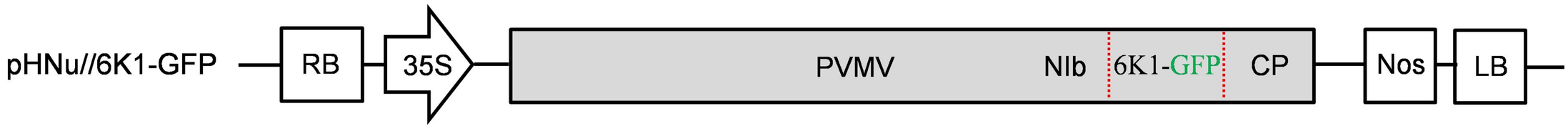

(B)

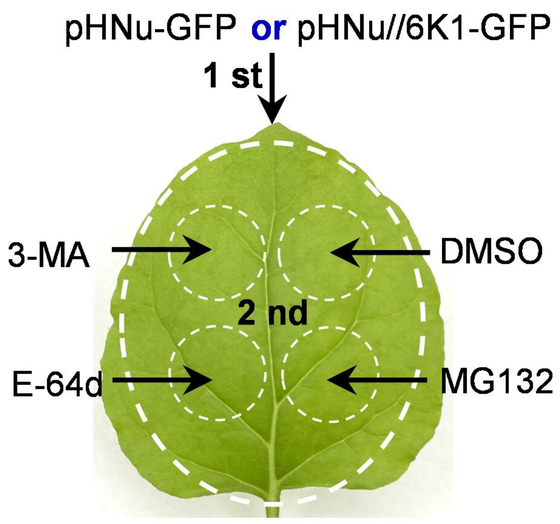

(C)

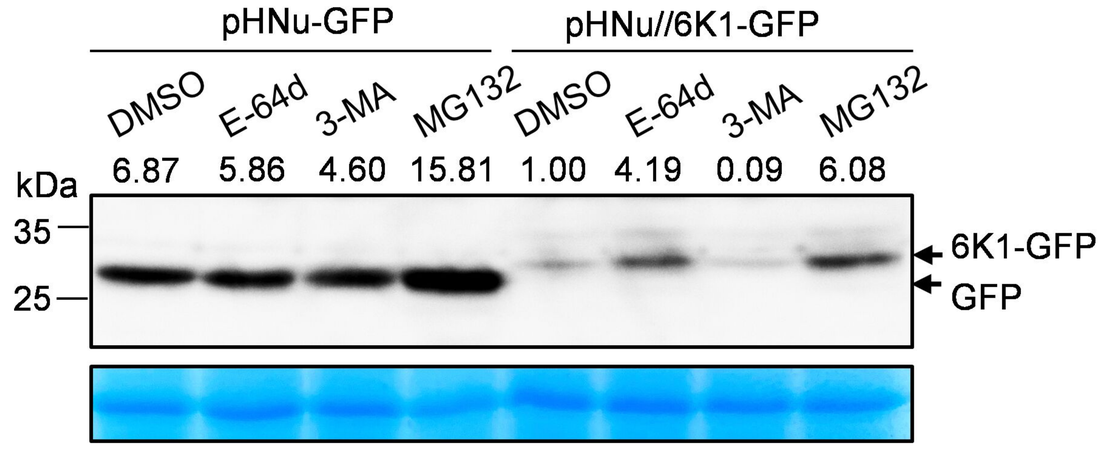

(D)

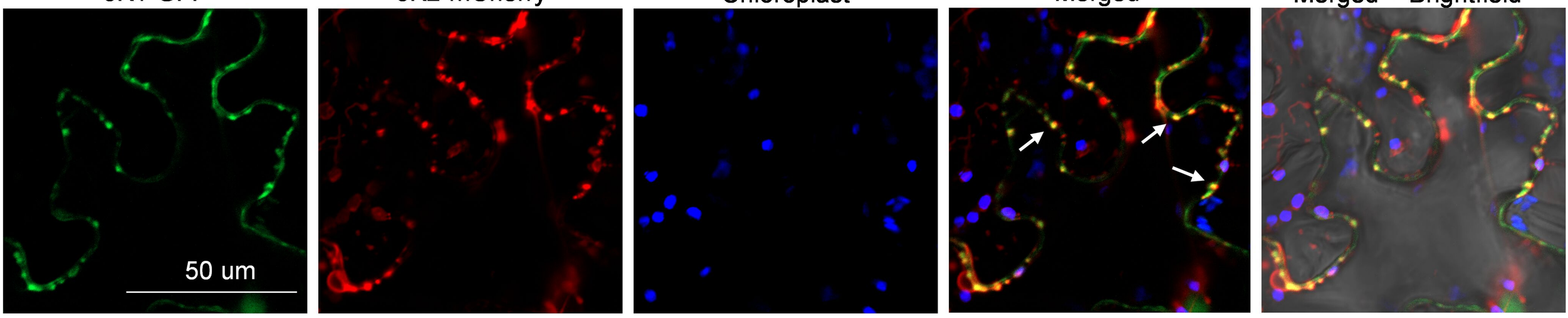

(E)

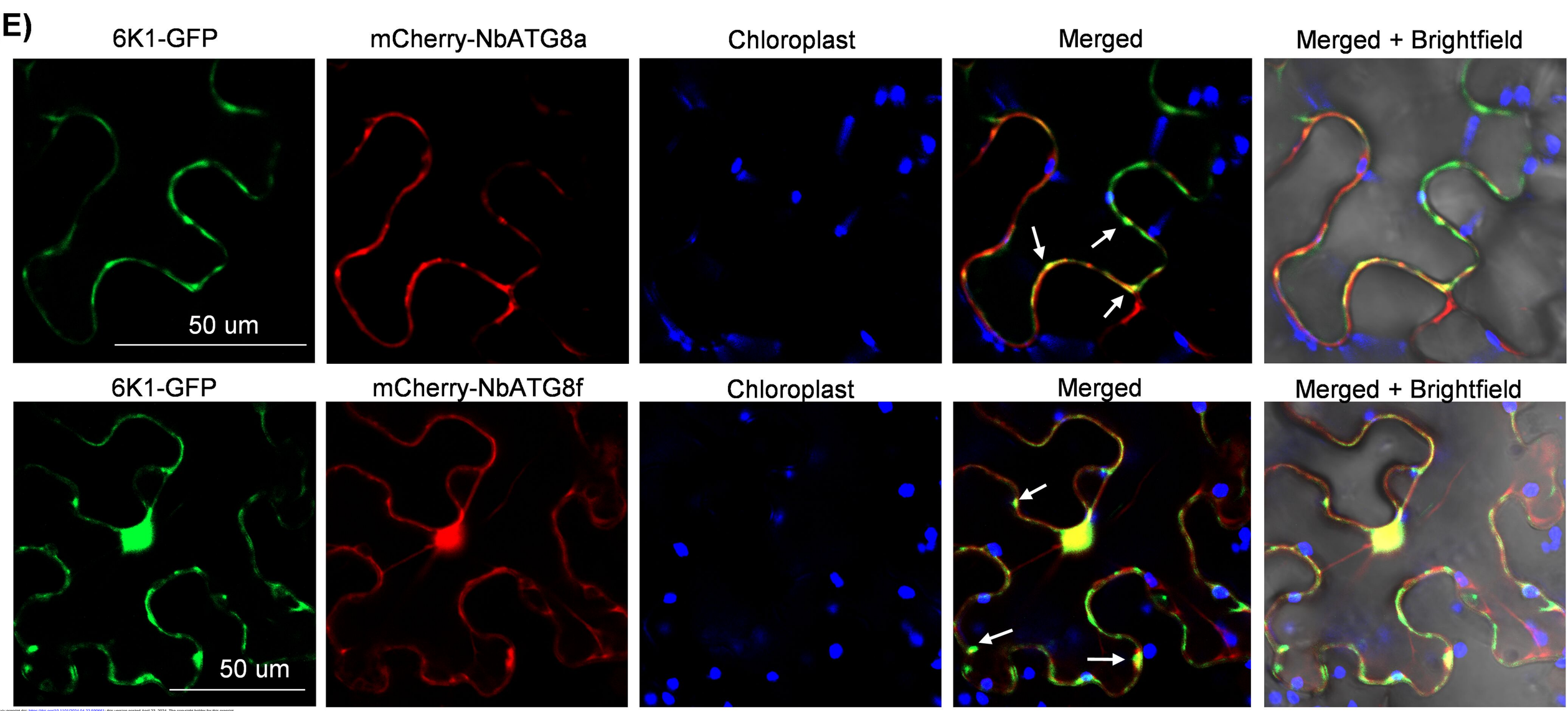

(F)

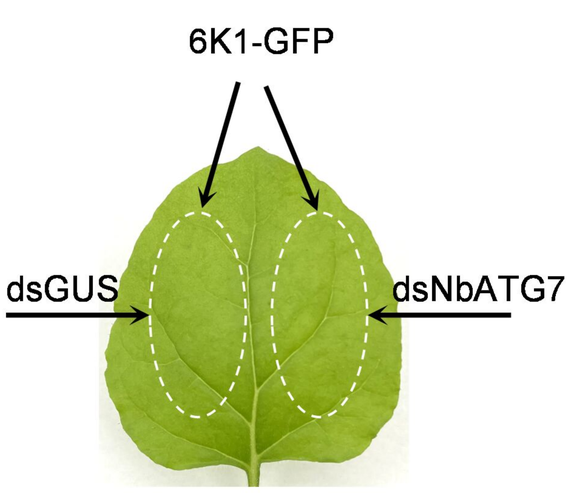

(G)

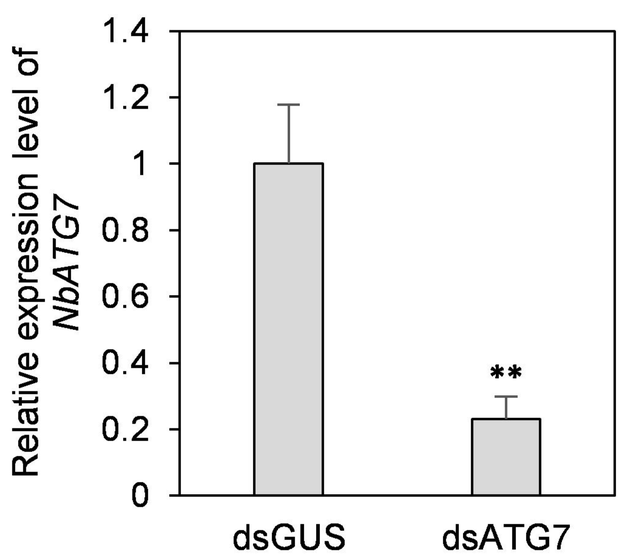

(H)

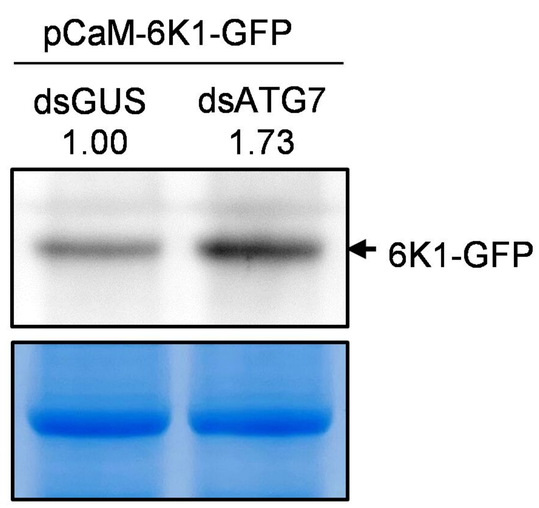

(A)

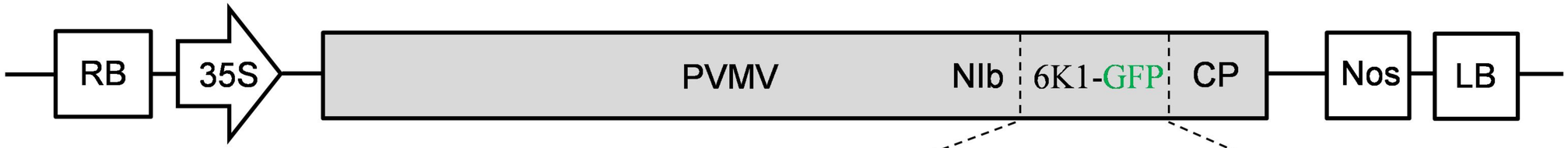

	30	32	34	36	39
pHNu//6K1-GFP	D	V	K	L	L
pHNu//6K1(D30A)-GFP	A	V	K	L	L
pHNu//6K1(V32A)-GFP	D	A	K	L	L
pHNu//6K1(K34A)-GFP	D	V	A	L	L
pHNu//6K1(L36A)-GFP	D	V	K	A	L
pHNu//6K1(L39A)-GFP	D	V	K	L	A

(B)

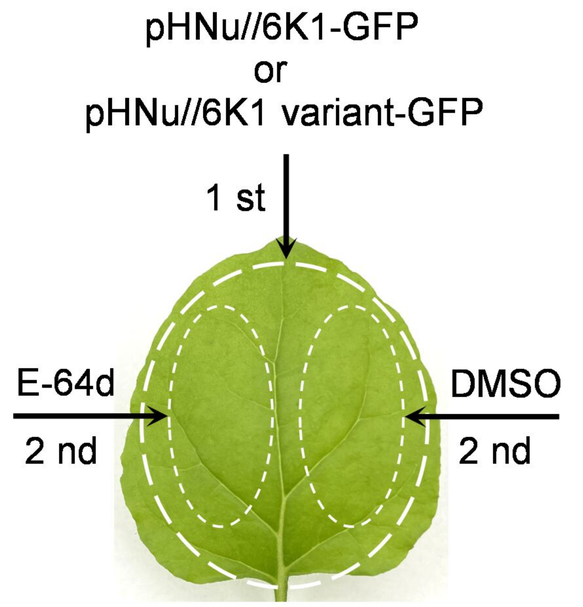

(C)

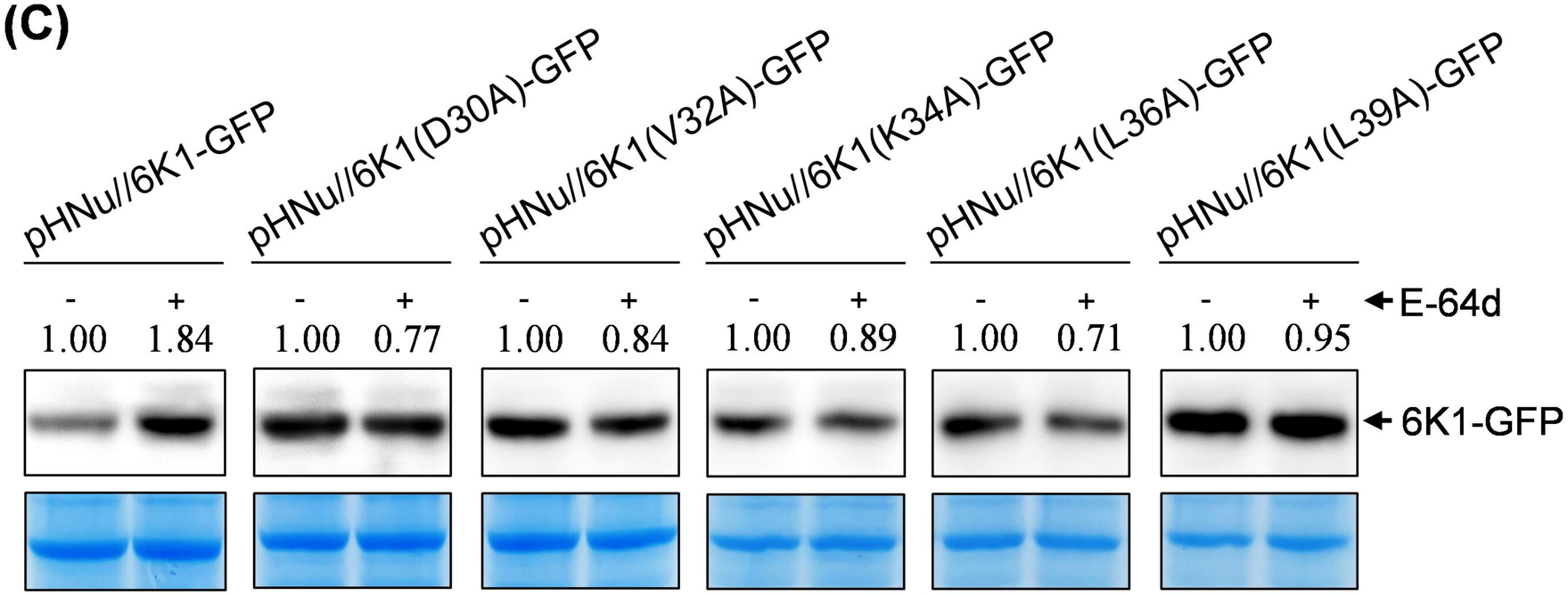

(D)

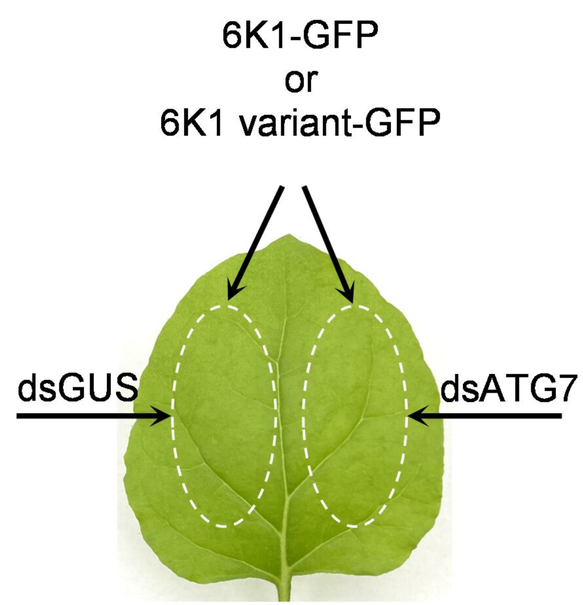

(E)